

Ultra-complex conductivity diagrams in the nearly free electron approximation

A.Ya. Maltsev

*L.D. Landau Institute for Theoretical Physics
142432 Chernogolovka, pr. Ak. Semenova 1A, maltsev@itp.ac.ru*

We investigate the possibility of the emergence of ultra-complex conductivity diagrams in the nearly free electron approximation for metals with cubic symmetry. Estimates show that the emergence of such diagrams requires the Fermi level to fall into very narrow energy intervals within the conduction band. In our view, this circumstance is mostly due to the high symmetry and the simplest analytical form of the dispersion relations $\epsilon(\mathbf{p})$ under consideration.

I. INTRODUCTION

In this paper, we consider the angular diagrams that determine the conductivity of normal metals in strong magnetic fields. We note that we are interested only in metals with sufficiently complex Fermi surfaces extending in all directions in \mathbf{p} -space (Fig. 1).

As is well known (see e.g. [1–4]), the electron quasi-momentum is defined modulo the vectors of the reciprocal lattice L^* :

$$\mathbf{p} \equiv \mathbf{p} + n_1 \mathbf{a}_1 + n_2 \mathbf{a}_2 + n_3 \mathbf{a}_3, \\ n_1, n_2, n_3 \in \mathbb{Z},$$

where the basis of the lattice L^* is given by the vectors

$$\mathbf{a}_1 = 2\pi\hbar \frac{\mathbf{l}_2 \times \mathbf{l}_3}{(\mathbf{l}_1, \mathbf{l}_2, \mathbf{l}_3)}, \quad \mathbf{a}_2 = 2\pi\hbar \frac{\mathbf{l}_3 \times \mathbf{l}_1}{(\mathbf{l}_1, \mathbf{l}_2, \mathbf{l}_3)}, \\ \mathbf{a}_3 = 2\pi\hbar \frac{\mathbf{l}_1 \times \mathbf{l}_2}{(\mathbf{l}_1, \mathbf{l}_2, \mathbf{l}_3)},$$

and $(\mathbf{l}_1, \mathbf{l}_2, \mathbf{l}_3)$ define the basis of the crystallographic lattice L .

As a consequence, the dispersion relation (the dependence of energy on quasi-momentum) $\epsilon(\mathbf{p})$ in a crystal can be considered either as a 3-periodic function in the space \mathbb{R}^3 or simply as a smooth function on the three-dimensional torus

$$\mathbb{T}^3 = \mathbb{R}^3 / L^*$$

determined by the factorization of \mathbf{p} -space by the reciprocal lattice vectors.

The Fermi surface of a metal

$$S_F : \epsilon(\mathbf{p}) = \epsilon_F$$

can also be viewed either as a 3-periodic surface in the \mathbf{p} -space (Fig. 1) or as a smooth compact surface embedded in \mathbb{T}^3 . We note here that both of these representations play very important role when considering electronic phenomena in strong magnetic fields.

Each compact (orientable) surface S_F has a topological genus g , which can take values $g = 0, 1, 2, 3, 4, \dots$ (Fig. 2, a).

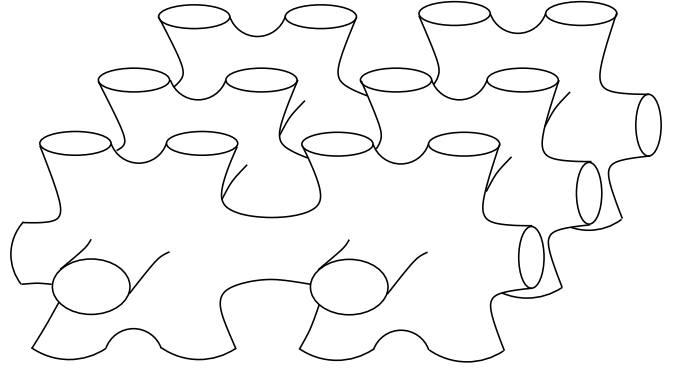


FIG. 1: Complex Fermi surface in \mathbf{p} -space.

The embedding $S_F \subset \mathbb{R}^3$ (and also $S_F \subset \mathbb{T}^3$) also has a topological rank $\text{Rank } S_F$. By definition, the topological rank of S_F determines the number of independent directions of extension of the surface S_F in \mathbb{R}^3 (Fig. 2, b). It is easy to see that the rank of the Fermi surface can take the values 0, 1, 2, and 3.

For topological reasons, the rank of a Fermi surface cannot exceed its genus. Thus, Fermi surfaces that are sufficiently complex from our point of view have $\text{Rank } S_F = 3$ and $g \geq 3$.

The application of an external magnetic field causes an adiabatic evolution of the electron states in a crystal, which is described by the quasi-momentum evolution determined by the system

$$\dot{\mathbf{p}} = \frac{e}{c} [\mathbf{v}_{\text{gr}}(\mathbf{p}) \times \mathbf{B}] \equiv \frac{e}{c} [\nabla \epsilon(\mathbf{p}) \times \mathbf{B}] \quad (\text{I.1})$$

Geometrically, the trajectories of system (I.1) are defined by the intersections of constant-energy surfaces

$$\epsilon(\mathbf{p}) = \text{const}$$

and planes orthogonal to \mathbf{B} . Electronic phenomena in metals are determined by trajectories of (I.1) lying on the Fermi surface $\epsilon(\mathbf{p}) = \epsilon_F$. As can be seen, for complex Fermi surfaces, the shape of the trajectories of (I.1) can strongly depend on the direction of \mathbf{B} (Fig. 3, a).

In the limit of large mean free paths and strong magnetic fields, electron transport phenomena in a crystal are

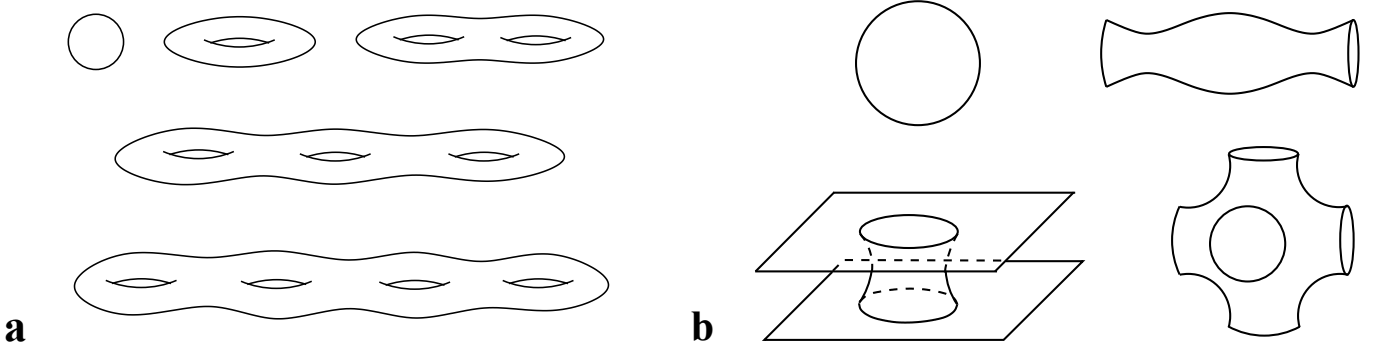


FIG. 2: (a) Abstract orientable surfaces of genus $g = 0, 1, 2, 3, 4$. (b) Examples of Fermi surfaces of rank 0, 1, 2 and 3.

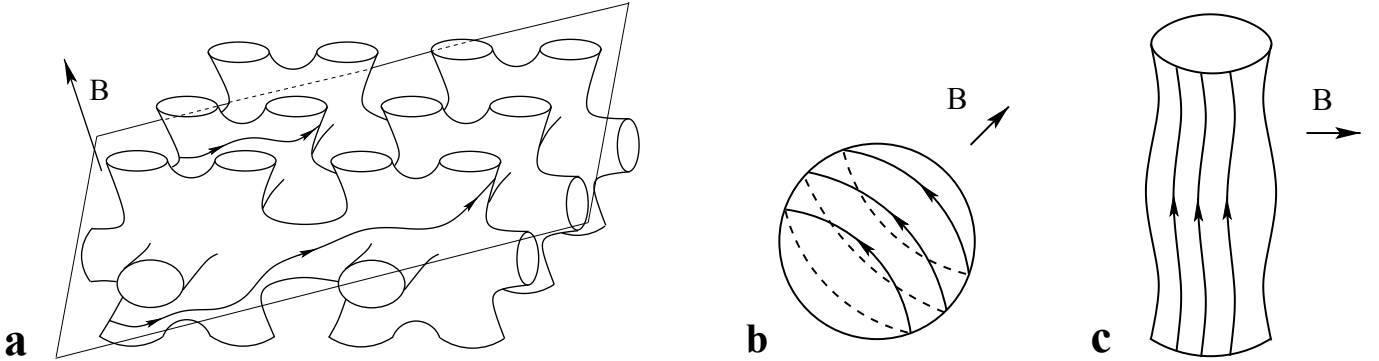


FIG. 3: (a) Trajectories of the system (I.1) on the Fermi surface of a rather complex shape. (b) Closed trajectories of the system (I.1). (c) Open periodic trajectories of the system (I.1).

largely determined by the geometry of the trajectories of system (I.1) in the \mathbf{p} -space. In particular, the behavior of the conductivity tensor $\sigma^{kl}(\mathbf{B})$ depends significantly on the presence or absence of open (unclosed) trajectories of system (I.1) on the Fermi surface ([5–8]). The corresponding limit can be formally written as the condition $\omega_B\tau \gg 1$, where ω_B is the cyclotron frequency, and τ is the electron mean free time in the crystal.

More precisely, it is necessary in fact to require that the electron travels a sufficiently large part of its trajectory (compared to p_F) between scattering events. It should be noted immediately that this limit applies to sufficiently pure single-crystal samples at low temperatures ($T \leq 1\text{K}$) and strong magnetic fields ($B \geq 1\text{Tl}$).

A striking example of the manifestation of the geometry of trajectories of (I.1) in transport phenomena is the difference in the contributions of closed and open periodic trajectories (Fig. 3, b, c) to the conductivity tensor in the limit $\omega_B\tau \rightarrow \infty$ ([5]).

$$\Delta\sigma_{\text{closed}}^{kl} \simeq \frac{ne^2\tau}{m^*} \begin{pmatrix} (\omega_B\tau)^{-2} & (\omega_B\tau)^{-1} & (\omega_B\tau)^{-1} \\ (\omega_B\tau)^{-1} & (\omega_B\tau)^{-2} & (\omega_B\tau)^{-1} \\ (\omega_B\tau)^{-1} & (\omega_B\tau)^{-1} & * \end{pmatrix}, \quad (\text{I.2})$$

$$\Delta\sigma_{\text{periodic}}^{kl} \simeq \frac{ne^2\tau}{m^*} \begin{pmatrix} (\omega_B\tau)^{-2} & (\omega_B\tau)^{-1} & (\omega_B\tau)^{-1} \\ (\omega_B\tau)^{-1} & * & * \\ (\omega_B\tau)^{-1} & * & * \end{pmatrix} \quad (\text{I.3})$$

It can be seen that the contribution of closed trajectories to the tensor $\sigma^{kl}(\mathbf{B})$ is similar to the contribution of the free electron gas, while the contribution (I.3) has a sharp anisotropy in the plane orthogonal to \mathbf{B} .

In formulas (I.2) - (I.3), the quantity n plays the role of the charge carrier concentration, and m^* is the effective electron mass in the crystal. The sign $*$ here denotes dimensionless constants of order 1.

Formulas (I.2) - (I.3) describe the asymptotic behavior of the tensor $\sigma^{kl}(B)$ in the limit $\omega_B\tau \rightarrow \infty$, in particular, each matrix element above is defined up to a constant factor of order 1. However, one important remark can be made.

Namely, if we are talking about the contribution of all closed trajectories covering the Fermi surface of the form Fig. 3b, then a more precise expression can be given for the Hall conductivity. Thus, in the leading order in $1/B$, the quantity $\sigma^{xy}(B)$ has the form ([1–4, 8])

$$\sigma^{xy} = -\sigma^{yx} = \pm \frac{ec}{B} \frac{2V}{(2\pi\hbar)^3}, \quad (\text{I.4})$$

where V is the volume bounded by the surface S_F in

the \mathbf{p} - space.

As can be seen, the value (I.4) does not depend on the direction of the magnetic field for a given value of B . The signs + and - in formula (I.4) correspond to the electron- and hole-type Fermi surfaces, respectively. Recall that for a dispersion relation $\epsilon(\mathbf{p})$, such that

$$\epsilon_{\min} \leq \epsilon(\mathbf{p}) \leq \epsilon_{\max},$$

the electron-type Fermi surfaces Fig. 3b arise at values ϵ_F close to ϵ_{\min} , and the hole-type Fermi surfaces arise at ϵ_F close to ϵ_{\max} .

Note also that for Fermi surfaces containing open trajectories of system (I.1), the relation (I.4) is not satisfied.

The problem of describing all possible trajectories of system (I.1) was posed by S.P. Novikov in his work [9] and was then intensively studied in his topological school ([10–17]). As a result of the research, a complete classification of all trajectories of systems (I.1) with arbitrary laws $\epsilon(\mathbf{p})$, as well as a detailed description of their geometric properties, was carried out. In addition, a description of all possible modes of conductivity behavior in the limit $\omega_B \tau \rightarrow \infty$, corresponding to open trajectories of various types, has also been obtained by now (see, for example, [18–20]).

For a metal with a given Fermi surface S_F , it is natural to introduce the “angular diagram” defined by the system (I.1). Namely, for each direction of \mathbf{B} :

$$\mathbf{n} = \mathbf{B}/B \in \mathbb{S}^2,$$

the angular diagram indicates the type of open trajectories (or their absence) on the surface S_F . Since each type of open trajectories on S_F is associated with a certain type of behavior of the tensor $\sigma^{kl}(B)$ as $\omega_B \tau \rightarrow \infty$, we will call such diagrams diagrams of conductivity in strong magnetic fields.

As is easy to see, for values ϵ_F close to ϵ_{\min} or ϵ_{\max} , the conductivity diagrams are very simple. Namely, all directions $\mathbf{n} \in \mathbb{S}^2$ correspond here to the presence of only closed trajectories on the Fermi surface (Fig. 3, b). The Hall conductivity here is given by the formula (I.4) and is of the electron type at $\epsilon_F \rightarrow \epsilon_{\min}$ and of the hole type at $\epsilon_F \rightarrow \epsilon_{\max}$.

We will also classify as simple diagrams those that allow only periodic open trajectories of (I.1) on the Fermi surface. As a rule, such diagrams also arise for values of ϵ_F that are “not too” distant from ϵ_{\min} or ϵ_{\max} .

The main type of open trajectories of (I.1) are stable open trajectories, i.e. trajectories that are stable with respect to all small rotations of \mathbf{B} , as well as small variations in the value of ϵ_F .

The stable open trajectories of system (I.1) have remarkable geometric properties ([10, 11, 13]). Namely:

1) Each stable open trajectory of system (I.1) lies (in a plane orthogonal to \mathbf{B}) in a straight strip of finite width, passing through it (Fig. 4, a).

2) The mean direction of stable open trajectories (in all planes orthogonal to \mathbf{B}) for a given direction of \mathbf{B} is

given by the intersection of the plane orthogonal to \mathbf{B} and some (“integer”) plane Γ generated by two reciprocal lattice vectors.

3) The plane Γ is unchanged for small rotations of \mathbf{B} and variations in the value of ϵ_F .

Note that, in general, stable open trajectories are not periodic.

The emergence of stable open trajectories on the Fermi surface corresponds to domains Ω_α (Stability Zones) on the angular diagram, each of which corresponds to its own integer plane Γ_α (Fig. 4, b). The Zones Ω_α , as well as the integer planes Γ_α , are experimentally observable, which formed the basis for the introduction of topological numbers in the conductivity of normal metals in [21].

Stable open trajectories can only appear on sufficiently complex Fermi surfaces (rank 2 or 3). We will classify an angular diagram as sufficiently complex if it contains Stability Zones Ω_α .

For a fixed dispersion relation $\epsilon(\mathbf{p})$, complex angular diagrams arise in some fixed energy range

$$\epsilon_F \in (\epsilon_1^A, \epsilon_2^A), \quad \epsilon_{\min} \leq \epsilon_1^A < \epsilon_2^A \leq \epsilon_{\max},$$

where the Fermi surfaces are sufficiently complex.

The interval $(\epsilon_1^A, \epsilon_2^A)$ can be divided into 3 intervals

$$(\epsilon_1^A, \epsilon_2^A) = (\epsilon_1^A, \epsilon_1^B) \cup [\epsilon_1^B, \epsilon_2^B] \cup (\epsilon_2^B, \epsilon_2^A)$$

(for generic dispersion relations), corresponding to different structures of the angular diagrams (see [22, 23]). This circumstance is connected, among other things, with different behavior of the Hall conductivity for different values of ϵ_F .

Namely, in the evolution of the angular diagrams for $\epsilon_F \in (\epsilon_1^A, \epsilon_2^A)$, from the emergence of the first Stability Zones Ω_α to their disappearance (Fig. 5), one can see that all the diagrams contain large regions corresponding to the presence of only closed trajectories on the Fermi surface. These regions occupy nearly the entire unit sphere for $\epsilon_F \rightarrow \epsilon_1^A$ or $\epsilon_F \rightarrow \epsilon_2^A$ (Fig. 5, a, f) and correspond to electron Hall conductivity in the first case, and to hole Hall conductivity in the second case.

In fact, formulas (I.4) can also be applied to complex Fermi surfaces, provided that they contain only closed trajectories of the system (I.1) and this property is preserved for (any) small rotations of \mathbf{B} . In this case, the formulas (I.4) take the form

$$\sigma^{xy} = -\sigma^{yx} = \pm \frac{ec}{B} \frac{2V_\mp}{(2\pi\hbar)^3}, \quad (I.5)$$

where V_- is the volume of the region

$$\epsilon(\mathbf{p}) < \epsilon_F,$$

and V_+ is the volume of the region

$$\epsilon(\mathbf{p}) > \epsilon_F$$

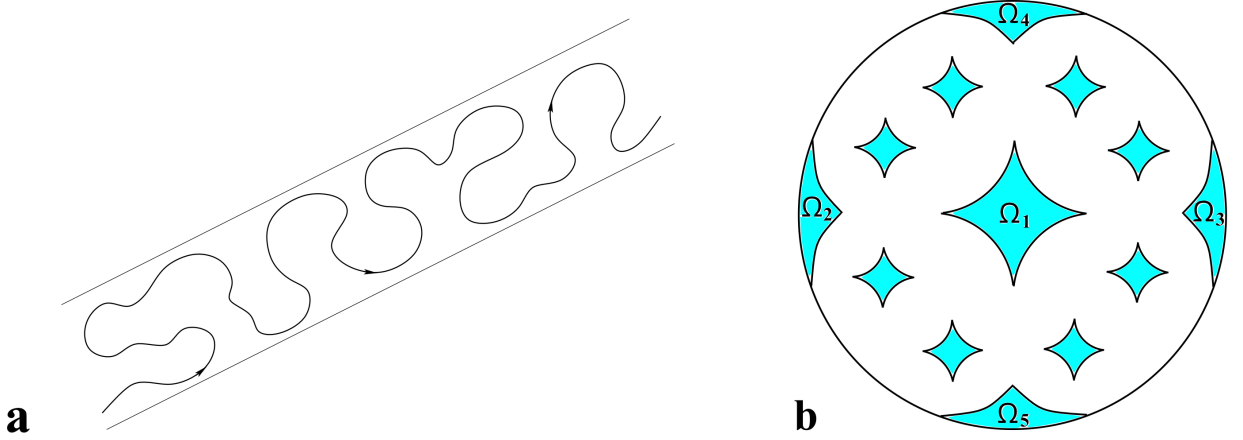


FIG. 4: (a) Stable open trajectory of system (I.1) in a plane orthogonal to \mathbf{B} . (b) Stability Zones corresponding to different integer planes Γ_α on the conductivity diagram (schematically).

in the torus

$$\mathbb{T}^3 = \mathbb{R}^3 / L^*$$

To select the value of V_- or V_+ in the formula (I.5), it is necessary to consider the picture of closed trajectories of (I.1) in planes orthogonal to \mathbf{B} . Namely, in the described situation, two cases are possible:

1) Situation $A(-)$:

A plane orthogonal to \mathbf{B} contains a unique unbounded component of the set

$$\epsilon(\mathbf{p}) > \epsilon_F ,$$

and all other components of the sets $\epsilon(\mathbf{p}) < \epsilon_F$ and $\epsilon(\mathbf{p}) > \epsilon_F$ are bounded (Fig. 6, a).

2) Situation $A(+)$:

A plane orthogonal to \mathbf{B} contains a unique unbounded component of the set

$$\epsilon(\mathbf{p}) < \epsilon_F ,$$

and all other components of the sets $\epsilon(\mathbf{p}) < \epsilon_F$ and $\epsilon(\mathbf{p}) > \epsilon_F$ are bounded (Fig. 6, b).

If the Fermi surface contains only closed trajectories of system (I.1), and this property is stable with respect to small rotations of \mathbf{B} , all planes orthogonal to \mathbf{B} have the same type ($A(-)$ or $A(+)$). In formula (I.5), the factor V_- corresponds to the situation $A(-)$, and the factor V_+ corresponds to the situation $A(+)$.

Near the edges of the interval $(\epsilon_1^A, \epsilon_2^A)$ the region

$$\mathbb{S}^2 \setminus \bigcup_\alpha \overline{\Omega_\alpha}$$

on the angular diagram is connected, and the number of Zones $\Omega_\alpha \subset \mathbb{S}^2$ is finite (Fig. 5, a, b, e, f). This type of angular diagrams persists in some intervals

$$\epsilon_F \in (\epsilon_1^A, \epsilon_1^B) \quad \text{and} \quad \epsilon_F \in (\epsilon_2^B, \epsilon_2^A) ,$$

where

$$\epsilon_1^A < \epsilon_1^B \leq \epsilon_2^B < \epsilon_2^A$$

Regions where only closed trajectories are present on the Fermi surface obviously correspond to electron Hall conductivity

$$\sigma^{xy} = -\sigma^{yx} = \frac{ec}{B} \frac{2V_-}{(2\pi\hbar)^3}$$

in the interval $\epsilon_F \in (\epsilon_1^A, \epsilon_1^B)$ and to hole Hall conductivity

$$\sigma^{xy} = -\sigma^{yx} = -\frac{ec}{B} \frac{2V_+}{(2\pi\hbar)^3}$$

in the interval $\epsilon_F \in (\epsilon_2^B, \epsilon_2^A)$.

We will call the conductivity diagrams diagrams of the type A_- for $\epsilon_F \in (\epsilon_1^A, \epsilon_1^B)$ and diagrams of the type A_+ for $\epsilon_F \in (\epsilon_2^B, \epsilon_2^A)$.

The interval $[\epsilon_1^B, \epsilon_2^B]$ separates the two types of diagrams described above (A_- and A_+). For generic dispersion relations $\epsilon(\mathbf{p})$, the interval $[\epsilon_1^B, \epsilon_2^B]$ has finite width ($\epsilon_2^B > \epsilon_1^B$).

In this paper, we will be interested in the position of the interval $[\epsilon_1^B, \epsilon_2^B]$ for the relations $\epsilon(\mathbf{p})$ arising in the nearly free electron approximation.

For $\epsilon_F \in (\epsilon_1^B, \epsilon_2^B)$ the set

$$\mathbb{S}^2 \setminus \bigcup_\alpha \overline{\Omega_\alpha}$$

contains regions of both electron and hole Hall conductivity (Fig. 5, c, d). Regions of different Hall conductivity are separated by “chains” of Zones Ω_α , which in generic case contain an infinite number of Zones. We will call angular diagrams of this type ultra-complex conductivity diagrams, or type B diagrams.

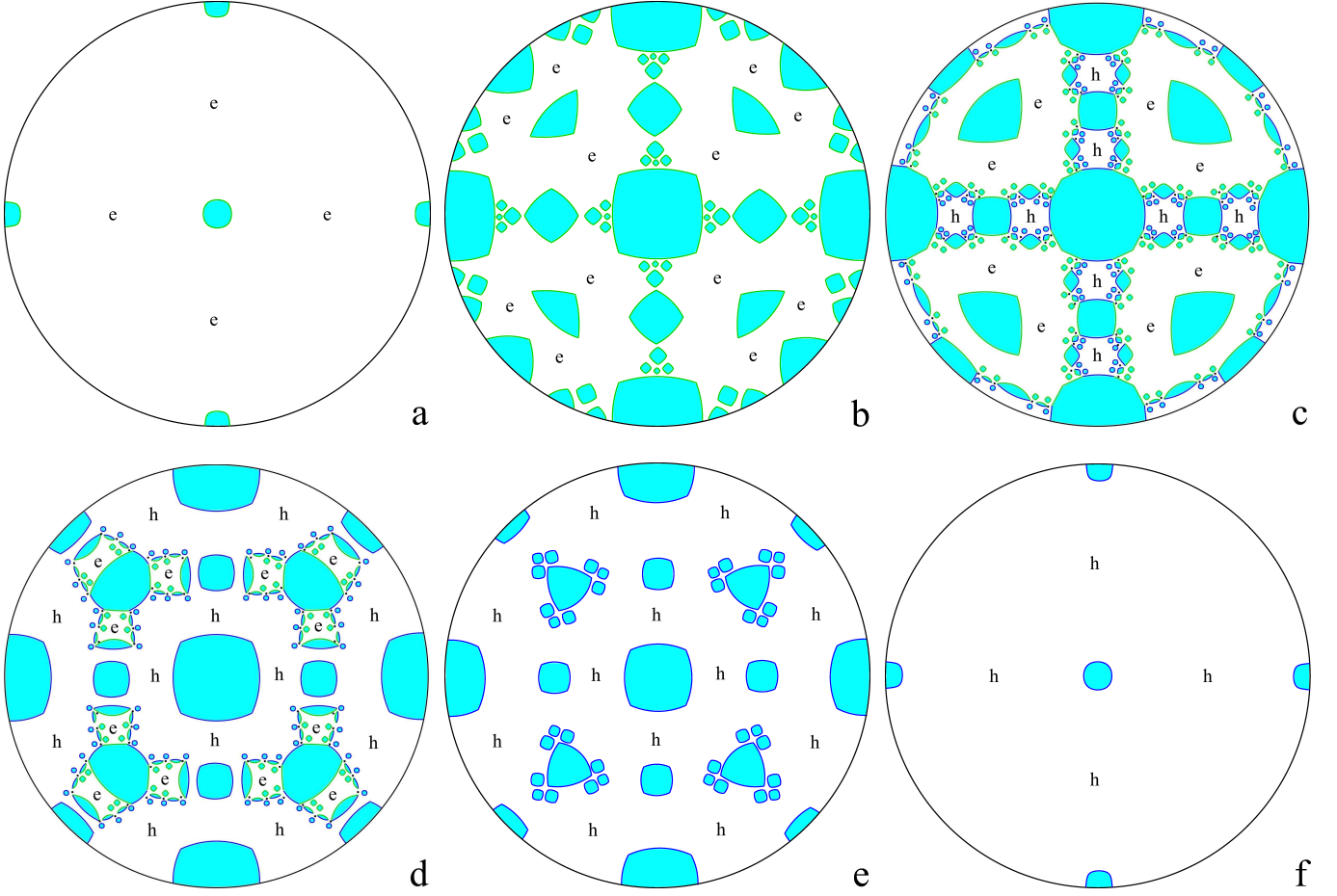


FIG. 5: Evolution of Stability Zones on the conductivity diagram in the interval $\epsilon_F \in (\epsilon_1^A, \epsilon_2^A)$ (schematically). The signs e and h mark the regions of electron and hole Hall conductivity, respectively.

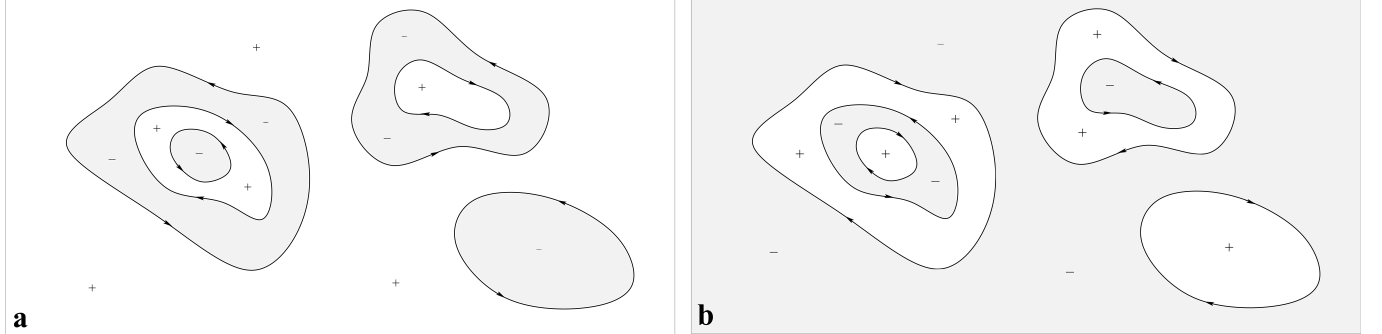


FIG. 6: Situations $A(-)$ and $A(+)$ in planes orthogonal to \mathbf{B} .

Generic diagrams of type B contain an infinite number of Zones Ω_α . Small Zones Ω_α correspond to increasingly complex geometry of the open trajectories of system (I.1) (Fig. 7, a), which, in turn, corresponds to increasingly complex behavior of the tensor $\sigma^{kl}(B)$ in the limit $\omega_B \tau \rightarrow \infty$.

The accumulation points of small Zones Ω_α repre-

sent special directions $\mathbf{n} \in \mathbb{S}^2$, corresponding to the emergence of trajectories called “chaotic”. The most common “chaotic” trajectories, or Dynnikov’s trajectories ([15, 16]), have a very complex shape, wandering “everywhere” in planes orthogonal to \mathbf{B} (Fig. 7, b). Trajectories of this type give the most complex contribution to the tensor $\sigma^{kl}(B)$, leading to the suppression of conduction.

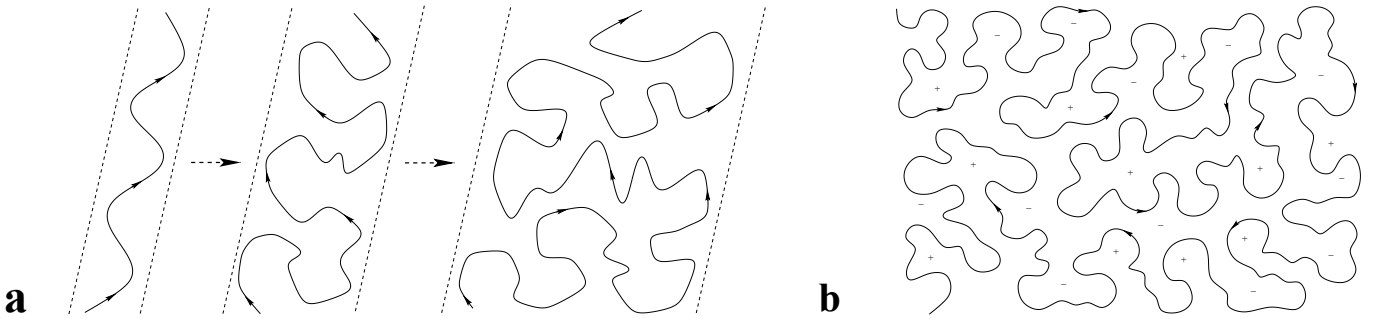


FIG. 7: (a) Complication of the shape of stable open trajectories for small Stability Zones Ω_α . (b) Dynnikov's "Chaotic" trajectory in a plane orthogonal to \mathbf{B} (schematically).

tivity along the direction of \mathbf{B} , as well as the emergence of fractional powers of $\omega_B \tau$ in the components $\sigma^{kl}(B)$ ([24, 25]). It should be noted that the study of chaotic trajectories of system (I.1) is actively continuing at the present time (see [26–43]).

As it turns out, the interval $[\epsilon_1^B, \epsilon_2^B]$ is usually quite narrow, and the probability of ϵ_F falling within it is quite low. This explains the difficulty of detecting of type B diagrams in real experiments. The paper [44] presents estimates for the position of the interval $[\epsilon_1^B, \epsilon_2^B]$ and its width in the tight-binding approximation. In this paper, we present estimates of the position of this interval in the nearly free electron approximation (see [1–4, 8, 45]) for crystals of cubic symmetry. The presented results can be useful both for searching for ultra-complex conductivity diagrams and, possibly, for obtaining them by external action on the sample.

II. ULTRA-COMPLEX ANGULAR DIAGRAMS AND THE CASE OF THE SIMPLE CUBIC LATTICE

To determine the location of ultra-complex angular diagrams, it is convenient to relate them to the angular diagrams of the entire dispersion relation $\epsilon(\mathbf{p})$. The angular diagram of a dispersion relation ([17]) specifies the interval $[\epsilon_1(\mathbf{n}), \epsilon_2(\mathbf{n})]$ of occurrence of open trajectories of system (I.1), as well as their type, for each direction \mathbf{B} for a given $\epsilon(\mathbf{p})$. According to [17]:

1) For each direction $\mathbf{n} = \mathbf{B}/B$, open trajectories of system (I.1) arise in a closed interval

$$\epsilon_F \in [\epsilon_1(\mathbf{n}), \epsilon_2(\mathbf{n})] ,$$

which can contract to a point

$$\epsilon_1(\mathbf{n}) = \epsilon_2(\mathbf{n}) = \epsilon_0(\mathbf{n})$$

2) The case $\epsilon_2(\mathbf{n}) > \epsilon_1(\mathbf{n})$ corresponds to the emergence of stable or periodic open trajectories of (I.1).

For directions \mathbf{n} of maximal irrationality, case (2) corresponds to the emergence of stable open trajectories of (I.1) that have the same mean direction for all

$\epsilon_F \in [\epsilon_1(\mathbf{n}), \epsilon_2(\mathbf{n})]$. The functions $\epsilon_1(\mathbf{n})$ and $\epsilon_2(\mathbf{n})$ are continuous on the set of directions \mathbf{n} of maximal irrationality and can be extended to continuous functions $\tilde{\epsilon}_1(\mathbf{n})$ and $\tilde{\epsilon}_2(\mathbf{n})$ on the unit sphere. The connected components of the set

$$\tilde{\epsilon}_2(\mathbf{n}) > \tilde{\epsilon}_1(\mathbf{n})$$

define Stability Zones W_α on \mathbb{S}^2 , corresponding to stable open trajectories associated with different integer planes Γ_α . Stability Zones W_α represent domains with piecewise smooth boundaries on the unit sphere ([17]).

The Zones W_α form a dense set on the unit sphere (Fig. 8); moreover, for dispersion laws satisfying the condition

$$\epsilon(\mathbf{p}) = \epsilon(-\mathbf{p}) ,$$

their union is a set of full measure on \mathbb{S}^2 (I.A. Dynnikov, P. Hubert, P. Mercat, A.S. Skripchenko, in preparation). The picture of Zones W_α and behavior of the functions $\tilde{\epsilon}_1(\mathbf{n})$, $\tilde{\epsilon}_2(\mathbf{n})$ (as well as $\epsilon_1(\mathbf{n})$ and $\epsilon_2(\mathbf{n})$) provide important general information about a relation $\epsilon(\mathbf{p})$.

Zones Ω_α (on the conductivity angular diagram) represent subdomains of Zones W_α , such that

$$\mathbf{n} \in W_\alpha , \quad \epsilon_F \in [\tilde{\epsilon}_1(\mathbf{n}), \tilde{\epsilon}_2(\mathbf{n})]$$

(if this set is not empty).

As can be seen, for the values of ϵ_1^A and ϵ_2^A we have the relations

$$\epsilon_1^A = \min_{\mathbb{S}^2} \tilde{\epsilon}_1(\mathbf{n}) , \quad \epsilon_2^A = \max_{\mathbb{S}^2} \tilde{\epsilon}_2(\mathbf{n})$$

For directions of \mathbf{B} of maximal irrationality, the condition $\epsilon_F < \tilde{\epsilon}_1(\mathbf{n})$ means falling into the region of the presence of only closed trajectories on the Fermi surface (on the conductivity diagram) with the Hall conductivity of the electron type. Similarly, the condition $\epsilon_F > \tilde{\epsilon}_2(\mathbf{n})$ for such directions of \mathbf{B} means falling into the region of the presence of only closed trajectories on the Fermi surface with the Hall conductivity of the hole type.

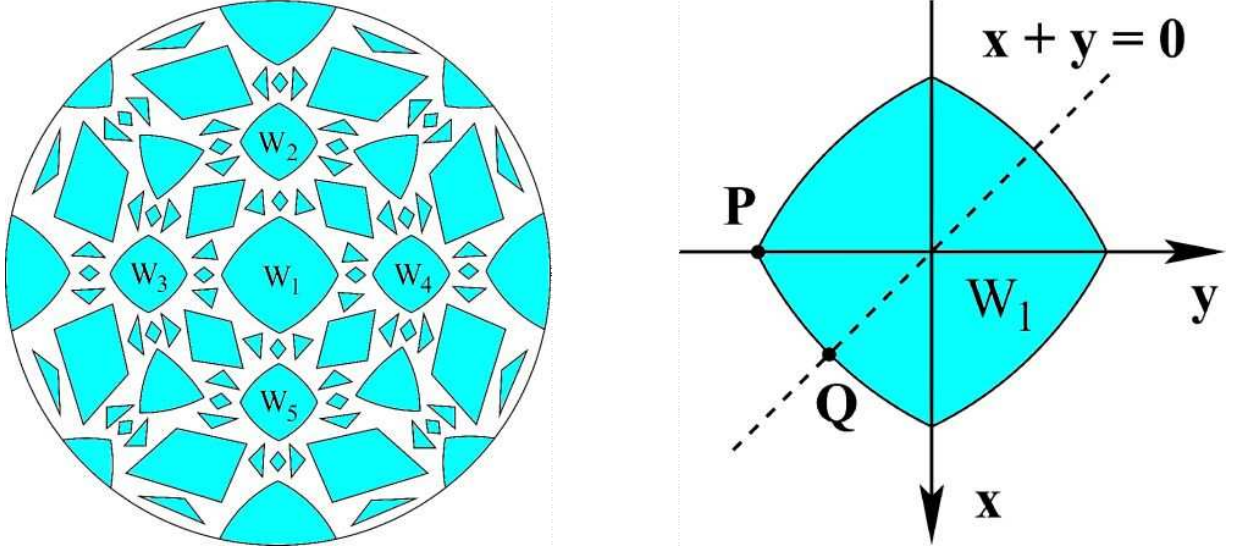


FIG. 8: Stability Zones W_α on the angular diagram for a dispersion relation $\epsilon(\mathbf{p})$ (schematically) and “symmetric” points P and Q on the boundary of Zone W_1 .

The presence of regions of both types on the conductivity angular diagram means the condition

$$\min_{\mathbb{S}^2} \tilde{\epsilon}_2(\mathbf{n}) < \epsilon_F < \max_{\mathbb{S}^2} \tilde{\epsilon}_1(\mathbf{n}) ,$$

that entails the relations

$$\epsilon_1^B = \min_{\mathbb{S}^2} \tilde{\epsilon}_2(\mathbf{n}) , \quad \epsilon_2^B = \max_{\mathbb{S}^2} \tilde{\epsilon}_1(\mathbf{n}) , \quad (\text{II.1})$$

which determine the interval of emergence of type B conductivity diagrams ([22, 23]).

Let us immediately note that for “physically realistic” dispersion relations we will assume that all Zones Ω_α and W_α are simply connected ([23]). This, in particular, implies the relations

$$\max_{W_\alpha} \tilde{\epsilon}_1(\mathbf{n}) = \max_{\partial W_\alpha} \tilde{\epsilon}_1(\mathbf{n}) , \quad \min_{W_\alpha} \tilde{\epsilon}_2(\mathbf{n}) = \min_{\partial W_\alpha} \tilde{\epsilon}_2(\mathbf{n})$$

for all Zones W_α (and their boundaries ∂W_α). The relations (II.1) can then be replaced by the relations

$$\epsilon_1^B = \min' \tilde{\epsilon}_2(\mathbf{n}) , \quad \epsilon_2^B = \max' \tilde{\epsilon}_1(\mathbf{n}) , \quad (\text{II.2})$$

where the minimum and maximum are taken only over the set of boundaries of W_α (and not over the entire unit sphere \mathbb{S}^2).

On the boundaries of W_α we have

$$\tilde{\epsilon}_1(\mathbf{n}) = \tilde{\epsilon}_2(\mathbf{n}) \equiv \tilde{\epsilon}_0(\mathbf{n}) ,$$

and thus the position of the interval $[\epsilon_1^B, \epsilon_2^B]$ is determined by the minimum and maximum of the function $\tilde{\epsilon}_0(\mathbf{n})$ over all boundaries of W_α :

$$\epsilon_1^B = \min_{\cup \partial W_\alpha} \tilde{\epsilon}_0(\mathbf{n}) , \quad \epsilon_2^B = \max_{\cup \partial W_\alpha} \tilde{\epsilon}_0(\mathbf{n})$$

For “physically realistic” relations $\epsilon(\mathbf{p})$, the location of ϵ_F in the interval $(\epsilon_1^B, \epsilon_2^B)$ entails a significant complication of conductivity diagrams compared to the case $\epsilon_F \notin (\epsilon_1^B, \epsilon_2^B)$. In particular, the regions of electron and hole Hall conductivity (and the presence of only closed trajectories on the Fermi surface) are divided on \mathbb{S}^2 by “quasi-one-dimensional” chains consisting of Zones Ω_α (Fig. 5, c, d). The number of Zones $\Omega_\alpha \subset \mathbb{S}^2$ for generic values $\epsilon_F \in [\epsilon_1^B, \epsilon_2^B]$ is infinite, which entails the emergence of stable open trajectories of arbitrarily complex shape (Fig. 7, a) for certain directions of \mathbf{B} . The accumulation points of Zones Ω_α correspond here, as a rule, to the emergence of chaotic trajectories (of the Tsarev or Dymnikov type) on the Fermi surface.

Finding the functions $\tilde{\epsilon}_0(\mathbf{n})$ is a complex problem requiring rather nontrivial calculations. Since we use here only some general approximation for the relations $\epsilon(\mathbf{p})$, our goal here will be to determine the interval $[\epsilon_1^B, \epsilon_2^B]$ with some (good) accuracy. For this purpose, we use here a technique proposed in the paper [44], which gives good (and in some cases accurate) estimates for the quantities ϵ_1^B and ϵ_2^B .

As we have already said, the interval $[\epsilon_1^B, \epsilon_2^B]$ is determined in our case by the values of $\tilde{\epsilon}_0(\mathbf{n})$ on the boundaries of the Zones W_α , i.e. on the set

$$\bigcup_{\alpha} \partial W_\alpha$$

For approximate evaluation of the interval $[\epsilon_1^B, \epsilon_2^B]$, we can consider the values $\tilde{\epsilon}_0(\mathbf{n})$ on the boundary of one of the largest Zones W_α , where the interval of values of $\tilde{\epsilon}_0(\mathbf{n})$ is sufficiently wide. For symmetric relations $\epsilon(\mathbf{p})$ such Zones are, as a rule, symmetric Zones W_α (the existence of which was proved in [17]). To calculate the

minimum and maximum of $\tilde{\epsilon}_0(\mathbf{n})$ on the boundary of such Zones, it is usually sufficient to calculate $\tilde{\epsilon}_0(\mathbf{n})$ at the most “symmetric” points ∂W_α (Fig. 8).

To determine the boundaries of the Zones W_α (as well as the values $\tilde{\epsilon}_0(\mathbf{n})$), it is necessary to consider the topological structure of system (I.1) on the surfaces

$$\epsilon(\mathbf{p}) = \text{const} ,$$

corresponding to the emergence of stable open trajectories ([10, 13, 17]). Namely, for any

$$\mathbf{n} \in W_\alpha , \quad \epsilon_F \in [\tilde{\epsilon}_1(\mathbf{n}), \tilde{\epsilon}_2(\mathbf{n})]$$

the surface $\epsilon(\mathbf{p}) = \epsilon_F$ represents a set of “carriers of open trajectories” separated by cylinders of closed trajectories of (I.1) (Fig. 9, a).

The carriers of stable open trajectories are periodically deformed integer planes (with holes) parallel to each other in \mathbb{R}^3 (Fig. 9, b) ([10, 13, 17]). A change in the topological structure of (I.1) on the surface S_F for directions $\mathbf{n} \in \partial \Omega_\alpha$ corresponds to the vanishing of the height of one of the cylinders of closed trajectories separating the carriers of open trajectories (Fig. 10).

The boundaries of Zones W_α correspond to the disappearance of at least two cylinders of closed trajectories of (I.1), which have different (electron and hole) types ([17]). The condition of the simultaneous disappearance of two cylinders of closed trajectories for

$$\mathbf{n} \in \partial W_\alpha , \quad \epsilon_F = \tilde{\epsilon}_0(\mathbf{n})$$

determines both the boundary of a Zone W_α and the values $\tilde{\epsilon}_0(\mathbf{n})$.

In general, studying the structure of system (I.1) on a Fermi surface is quite non-trivial and requires extensive computations (see, e.g., [15, 41, 43]). This study is significantly simplified for symmetric Zones W_α , where such a structure becomes more obvious. The use of “symmetric” points on the boundaries of such Zones makes it most convenient to find both their positions on \mathbb{S}^2 and the corresponding values $\tilde{\epsilon}_0(P, Q)$.

Below we illustrate our scheme using the example of the simple cubic lattice, which represents the simplest of the cases considered here.

The case of the simple cubic lattice is the simplest from the geometric point of view. The reciprocal lattice here is also simple cubic; we will assume its edge length to be equal to 2. As we have already said, we will consider the dispersion relations $\epsilon(\mathbf{p})$, obtained in the nearly free electron approximation.

Our goal is to determine the position of the interval $[\epsilon_1^B, \epsilon_2^B]$ within the interval $[\epsilon_{\min}, \epsilon_{\max}]$ and to estimate its width in comparison with the conduction band width. Based on this, we can normalize the values of ϵ and p such that

$$\epsilon = p^2$$

near the value $\mathbf{p} = (0, 0, 0)$.

The evolution of the Fermi surface for $\epsilon_F > 0$ begins with the emergence of growing spheres with centers at even integer points (Fig. 11, a) in \mathbb{R}^3 with their subsequent surgery upon the formation of intersections (Fig. 11, b).

The Fermi surface first becomes extended in the entire \mathbf{p} -space at $\epsilon_F = 1$, this is also the value after which stable open trajectories of system (I.1) ($\epsilon_1^A = 1$) first appear on it.

For values $\epsilon_F \in (1, 2)$ ($p_F \in (1, \sqrt{2})$), the Fermi surface contains a connected component extending in all directions in \mathbf{p} -space, as well as a periodic set of compact components (Fig. 11, b). It is easy to see that among the compact components there are only 3 nonequivalent ones, and the total number of connected components of the Fermi surface in $\mathbb{T}^3 = \mathbb{R}^3 / L^*$ is equal to 4.

In fact, the emergence of new components of the Fermi surface corresponds to the creation of the second conduction band with $\epsilon_{\min}^{(2)} = 1$. In the interval $\epsilon \in (1, 2)$ we must therefore consider the unbounded component to be the Fermi surface of the first conduction band (with $\epsilon_{\min}^{(1)} = 0$), and the 3 compact components to be the Fermi surface of the second band (with $\epsilon_{\min}^{(2)} = 1$).

At $\epsilon_F = 2$, the Fermi surface of the first band decomposes into compact components of rank 0 (equivalent to each other), which disappear (contract into points) at $\epsilon_F = 3$ (Fig. 11, c). Thus, for the first conduction band we have

$$\epsilon_{\min}^{(1)} = 0 , \quad \epsilon_{\max}^{(1)} = 3$$

The Fermi surface of the second band acquires rank 3 in the interval $\epsilon \in (2, 3)$ ($p \in (\sqrt{2}, \sqrt{3})$), extending in all directions in \mathbf{p} -space. For $\epsilon = 3$ the Fermi surface of the second band decomposes into components of rank zero, which vanish at the value $\epsilon = 4$ ($p = 2$). We thus have for the second conduction band

$$\epsilon_{\min}^{(2)} = 1 , \quad \epsilon_{\max}^{(2)} = 4$$

At the same time, for $\epsilon = 2$ ($p = \sqrt{2}$), new components of rank 0 are split off from the Fermi surface of the second conduction band, forming the Fermi surfaces of the following conduction bands, etc. (according to [45], each point in \mathbf{p} -space that falls inside n different spheres for a given ϵ_F represents filled states for the n first conduction bands). Continuing the procedure, we thus obtain an infinite set of (overlapping) energy bands (conduction bands).

At all points of \mathbf{p} -space we have the relations

$$\epsilon^{(s+1)}(\mathbf{p}) \geq \epsilon^{(s)}(\mathbf{p}) ,$$

at the same time

$$\epsilon^{(s+1)}(\mathbf{p}) = \epsilon^{(s)}(\mathbf{p})$$

at the intersections of the Fermi surfaces.

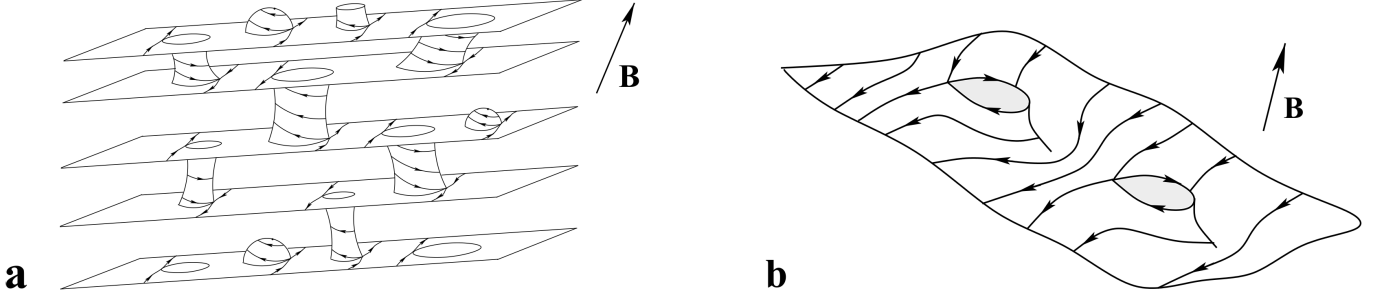


FIG. 9: (a) The Fermi surface cut by the cylinders of closed trajectories of (I.1) (schematically). (b) A carrier of stable open trajectories of system (I.1) in the full \mathbf{p} - space.

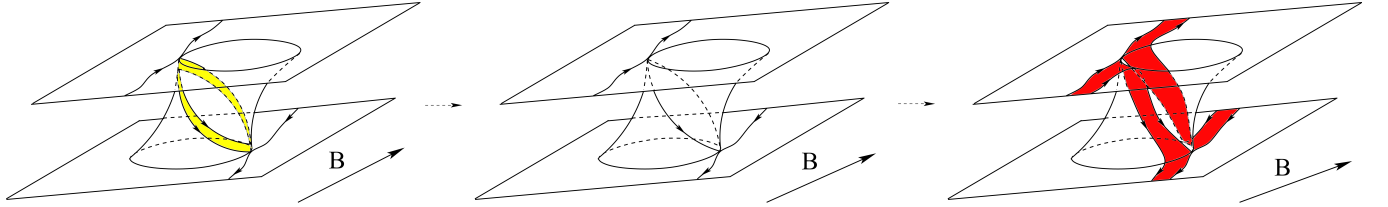


FIG. 10: The vanishing of the height of a cylinder of closed trajectories at the boundary of a Zone Ω_α and the destruction of a “stable” topological structure of system (I.1) on the Fermi surface (the occurrence of “jumps” between the carriers of open trajectories).

As is well known, in real nearly free electron approximation, the last equality is removed due to the (small) splitting of energy levels at the intersection of spectra. The Fermi surfaces are then smoothed out at the intersections, leading to the relations

$$\epsilon^{(s+1)}(\mathbf{p}) > \epsilon^{(s)}(\mathbf{p})$$

Our results here, however, are approximate (and, in particular, do not take into account deviations from the nearly free-electron approximation in real metals). Therefore, we will also consider here the shape of the Fermi surfaces as described above.

Here we will estimate the position of the interval $[\epsilon_1^B, \epsilon_2^B]$ for the first conduction band described above. As we have already said, we use here the values $\tilde{\epsilon}_0(\mathbf{n})$ at those points of ∂W_α where we can expect them to differ from each other the most. As such values, we can use the values $\tilde{\epsilon}_1(\mathbf{n}) = \tilde{\epsilon}_2(\mathbf{n}) = \tilde{\epsilon}_0(\mathbf{n})$ on the boundaries of the largest (symmetric) Stability Zones $W_\alpha \subset \mathbb{S}^2$. Here (and further) we will use the symmetric Zone W_1 , containing the direction $\mathbf{n} = (0, 0, 1)$ (Fig. 8).

The boundary points of the Zone W_1 are determined by the disappearance of two cylinders of closed trajectories of (I.1), dividing the Fermi surface into carriers of open trajectories for $\mathbf{n} \in W_1$. For the first conduction band, we obviously have

$$\epsilon_1^A = 1, \quad \epsilon_2^A = 2,$$

so that it suffices to consider the Fermi surfaces only for $\epsilon_F \in (1, 2)$. For $\mathbf{n} \in W_1$, the corresponding cylinders

of closed trajectories are shown in Fig. 12. To estimate the values ϵ_1^B and ϵ_2^B we use here the values of $\tilde{\epsilon}_0(\mathbf{n})$ at “symmetric” points P and Q on the boundary of W_1 shown in Fig. 8.

Let the radius of the circle arising at the intersection of the spheres for $1 < \epsilon_F < 2$ be r . The disappearance of the cylinder C_1 at the point P corresponds to the picture in the plane $\Pi \perp \mathbf{B}$ (passing through the point $(0, 0, 1) \in \mathbb{R}^3$) shown in Fig. 13, a. The projection of the plane Π onto the plane yz is a straight line with an inclination angle α such that

$$\tan \alpha = 1 - r$$

(Fig. 13, b).

The disappearance of the cylinder C_2 at the point P corresponds to the picture in the plane $\Pi \perp \mathbf{B}$ (passing through the point $(1, 1, 0) \in \mathbb{R}^3$), shown in Fig. 14, a. The projection of the plane Π onto the plane yz is a straight line with an inclination angle α such that

$$\sin \alpha = r$$

(Fig. 14, b).

From the condition of the simultaneous disappearance of the cylinders C_1 and C_2

$$1 - r = \frac{r}{\sqrt{1 - r^2}}$$

we then obtain $r \simeq 0.469$ and, accordingly,

$$\tilde{\epsilon}_0(P) = 1 + r^2 \simeq 1.22$$

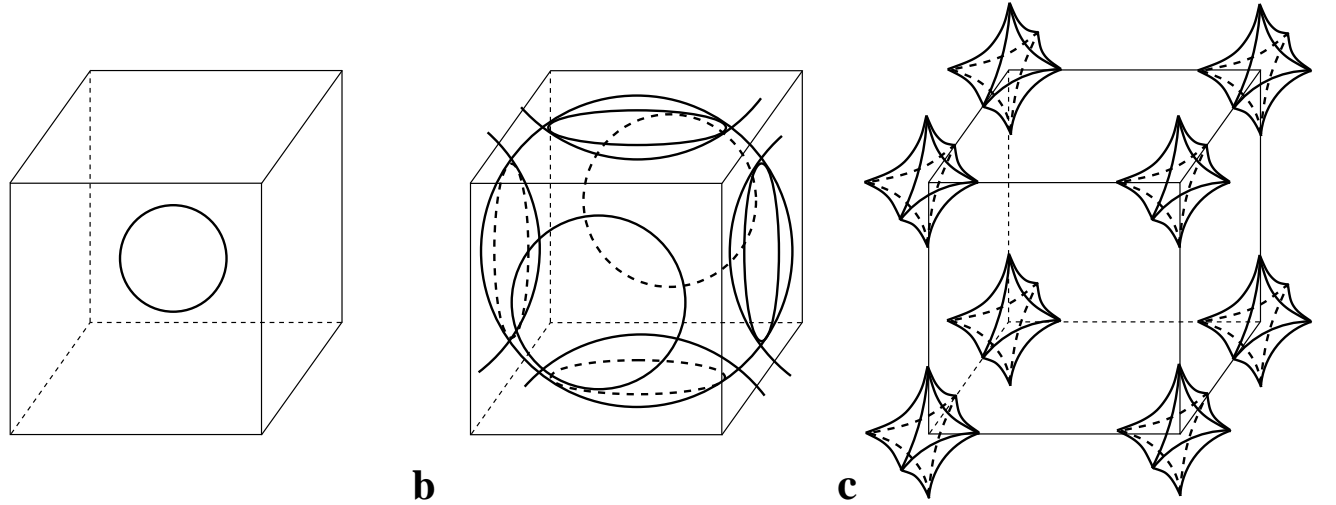


FIG. 11: (a) Emergence of the components of the Fermi surface of the first conduction band at $\epsilon_F > 0$. (b) Growth and surgery of the Fermi surface of the first conduction band at $\epsilon_F > 0$. (c) Disappearance of the components of the Fermi surface of the first conduction band at $\epsilon \rightarrow 3$ (simple cubic lattice).

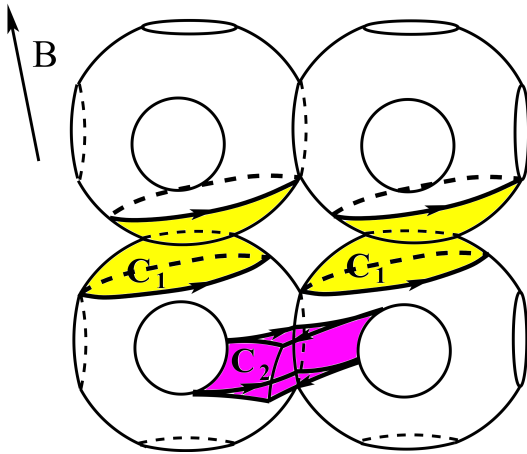


FIG. 12: The Fermi surface of the first conduction band for $\epsilon_F \in (1, 2)$ and the cylinders of closed trajectories of the electron (C_1) and hole (C_2) types for $\mathbf{n} \in W_1$ (simple cubic lattice).

The disappearance of the cylinder C_1 at $\mathbf{n} = Q$ corresponds to the position of the plane $\Pi \perp \mathbf{B}$ (passing through the point $(0, 0, 1) \in \mathbb{R}^3$), shown in Fig. 15, a. As is easy to see, the angle between the directions \mathbf{n} and z is determined by the relation

$$\tan \alpha = \sqrt{2} \tan \alpha' ,$$

where α' is the angle shown in Fig. 15, b. As is easy to show,

$$\tan \alpha' = \frac{\sqrt{2 - r^2} - r}{\sqrt{2 - r^2} + r}$$

The disappearance of the cylinder C_2 at $\mathbf{n} = Q$ corresponds to the position of the plane $\Pi \perp \mathbf{B}$ (passing through the point $(1, 1, 0) \in \mathbb{R}^3$), shown in Fig. 16, a. The angle between the directions \mathbf{n} and z is determined by the relation

$$\tan \alpha = \sqrt{2} \tan \alpha' = \sqrt{2} \frac{r}{\sqrt{1 - r^2}}$$

The condition

$$\frac{\sqrt{2 - r^2} - r}{\sqrt{2 - r^2} + r} = \frac{r}{\sqrt{1 - r^2}}$$

gives the value $r = 1/\sqrt{5}$ and, accordingly,

$$\tilde{\epsilon}_0(Q) = 1 + r^2 = 1.2$$

Thus, using our estimate, we obtain

$$[\epsilon_1^B, \epsilon_2^B] \simeq [1.2, 1.22]$$

for the first conduction band.

Abstracting from the normalization we use, we can also say that the interval of emergence of ultra-complex angular diagrams occurs near the value $0.4 \epsilon_{\max}$ from the bottom of the conduction band, and its length is $\simeq 0.7\%$ of the width of the conduction band.

Note also that the tight-binding approximation gives the zero width of the interval $[\epsilon_1^B, \epsilon_2^B]$ in the leading order for the simple cubic lattice (see e.g. [44]), and a nonzero width of $[\epsilon_1^B, \epsilon_2^B]$ appears there only in higher corrections. The nearly free electron approximation, as can be seen, differs from the tight-binding model at this point.

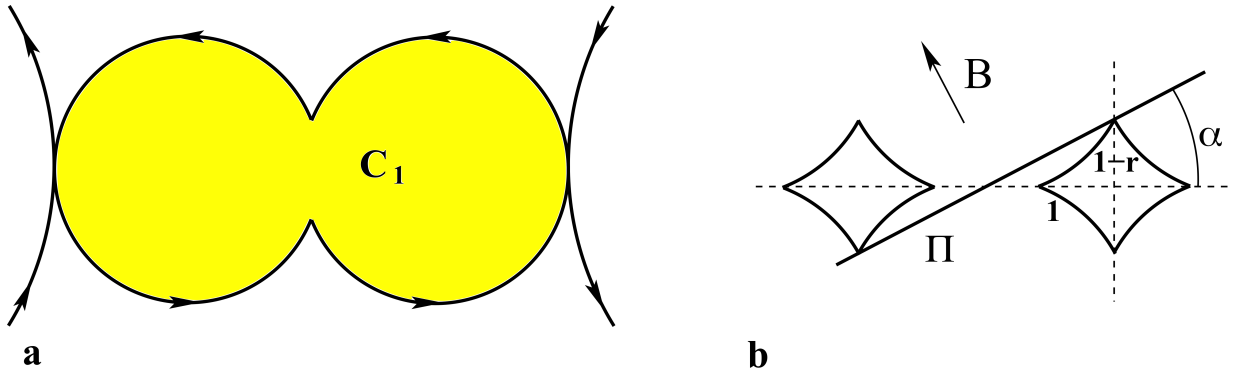


FIG. 13: (a) Cylinder C_1 of zero height in the plane $\Pi \perp \mathbf{B}$ passing through the point $(0, 0, 1)$ ($\mathbf{n} = P$); (b) Projection of the plane Π onto the plane yz (simple cubic lattice).

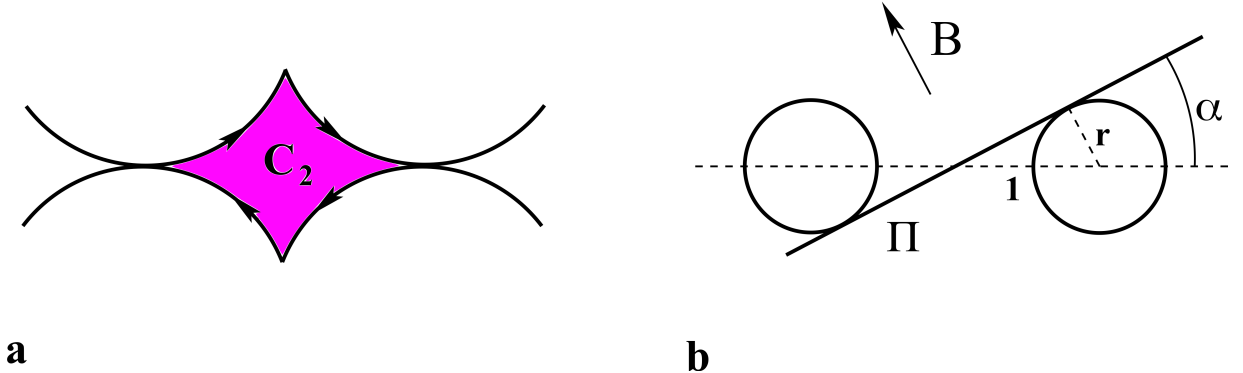


FIG. 14: (a) Cylinder C_2 of zero height in the plane $\Pi \perp \mathbf{B}$ passing through the point $(1, 1, 0)$ ($\mathbf{n} = P$); (b) Projection of the plane Π onto the plane yz (simple cubic lattice).

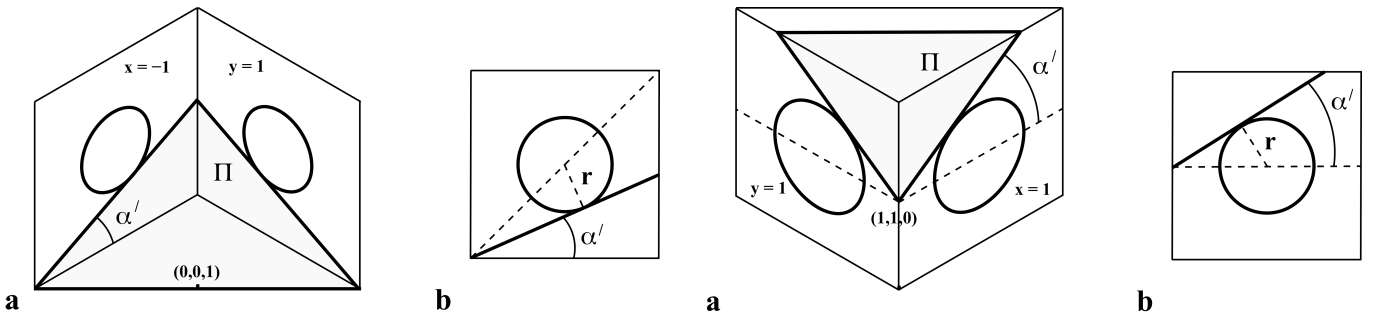


FIG. 15: (a) The position of the plane $\Pi \perp \mathbf{B}$ passing through the point $(0, 0, 1)$ at $\mathbf{n} = Q$ (cube interior shown); (b) The intersection of the plane $x = -1$ by the plane Π and angle α' ($\tan \alpha = \sqrt{2} \tan \alpha'$, simple cubic lattice).

III. THE FACE-CENTERED CUBIC LATTICE

Let's consider the case of the face-centered cubic lattice. The reciprocal lattice in this case is body-centered cubic. As in the previous case, we will assume its edge length to be equal to 2.

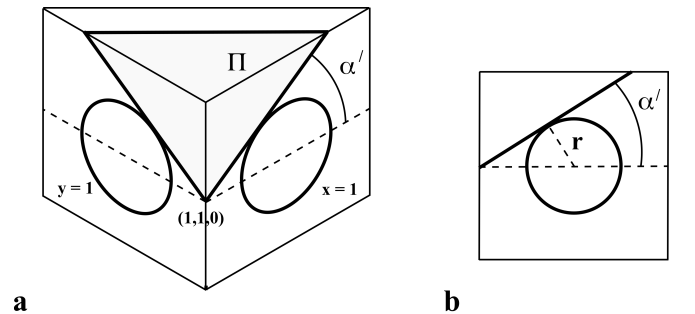


FIG. 16: (a) The position of the plane $\Pi \perp \mathbf{B}$ passing through the point $(1, 1, 0)$ at $\mathbf{n} = Q$ (the exterior of the cube is shown); (b) The intersection of the plane $x = 1$ by the plane Π and the angle α' ($\tan \alpha = \sqrt{2} \tan \alpha'$, simple cubic lattice).

The first Fermi surfaces are born near integer points $\mathbf{p} = (n, m, l)$, all of whose coordinates are either even or odd. Near these points, as in the previous section, we will assume

$$\epsilon(\mathbf{p}) = (\Delta \mathbf{p})^2$$

As in the previous case, we will carry out here an estimate of the position of the interval $[\epsilon_1^B, \epsilon_2^B]$ for the first conduction band.

As is well known, the Brillouin zone in this case is a truncated octahedron and has the shape shown in Fig. 17, a. The bottom of the first conduction band in our normalization obviously corresponds to the value $\epsilon_{\min} = 0$. The upper edge of the first conduction band corresponds to the values

$$\epsilon_{\max} = \frac{13}{9}, \quad p_{\max} = \sqrt{1 + \left(\frac{2}{3}\right)^2}$$

(Fig. 17, a).

Up to the value

$$\epsilon_F = \epsilon_1^A = \frac{3}{4}$$

the Fermi surface is a sphere. At $\epsilon_F = \epsilon_1^A = 3/4$ the spheres first touch each other ($p_1^A = \sqrt{3}/2$, Fig. 17, b), the Fermi surface acquires genus 4, and open trajectories first appear on it.

After the value

$$\epsilon_F = \epsilon^g = 1$$

($p^g = 1$) the genus of the Fermi surface increases to 7.

After the value

$$\epsilon_F = \epsilon_2^A = \frac{11}{9}, \quad p_2^A = \sqrt{1 + \left(\frac{\sqrt{2}}{3}\right)^2}$$

the Fermi surface breaks down into 6 compact components that look like "dumbbells".

After the value

$$\epsilon_F = \epsilon' = \frac{25}{18}, \quad p' = \frac{5}{6}\sqrt{2}$$

the "dumbbells" disintegrate into "balls" of the hole type, which then disappear at $\epsilon_F = \epsilon_{\max}$.

Let us now consider the projection of our Fermi surface onto the yz plane. The circles arising at the intersection of the spheres are now projected onto ellipses with semi-axes r and $r/\sqrt{3}$ (Fig. 18). It is also easy to construct projections of the cylinders C_1 , C_2 and C_3 onto the yz plane for $\mathbf{B} \parallel z$ (Fig. 18). As in the previous section, the cylinders C_1 , C_2 , and C_3 cut the Fermi surface into carriers of open trajectories \mathbb{T}_1^2 , \mathbb{T}_2^2 for $\mathbf{n} \in W_1$. Note here that the cylinder C_1 has a circular shape, while the cylinders C_2 and C_3 have "corners", like the cylinder C_2 in the previous section.

As can be seen, the disappearance of the cylinders C_1 , C_2 and C_3 for the direction $\mathbf{n} = P$ (Fig. 8) corresponds to the situation when the straight line passing through the point $(0, 0)$ (the projection of the plane orthogonal to \mathbf{B}) is tangent to both ellipses S_1 and S_2 shown in Fig. 18. This condition, as is easy to see, uniquely determines the quantity r , and also the value $\tilde{\epsilon}_0(P) = 3/4 + r^2$.

It is easy to verify that the equations of the ellipses S_1 and S_2 shown in Fig. 18 have the form

$$(y - z)^2 + 3(y + z - 1)^2 = 2r^2$$

and

$$3(y - z - 1)^2 + (y + z - 2)^2 = 2r^2$$

respectively.

The condition of tangency of the ellipse S_1 is

$$2(1 - \tan \alpha)^2 r^2 + 6(1 + \tan \alpha)^2 r^2 = 3(1 - \tan \alpha)^2,$$

and of the ellipse S_2 is

$$6(1 - \tan \alpha)^2 r^2 + 2(1 + \tan \alpha)^2 r^2 = 3(3 \tan \alpha - 1)^2,$$

which gives

$$r^2(P) \simeq 0.066885$$

and

$$\tilde{\epsilon}_0(P) \simeq 0.816885$$

For the angle of inclination of \mathbf{B} to the axis z , corresponding to the point P on the angular diagram, we have

$$\tan \alpha_P \simeq 0.45541$$

Let us now consider the direction $\mathbf{n} = Q$ (Fig. 8). When projected onto the plane $x + y = 0$, half of the circles S_i are transformed into segments of length $2r$, and the other half into ellipses with semi-axes r and $r\sqrt{2/3}$ (Fig. 19). The disappearance of the cylinders C_1 , C_2 and C_3 is now determined by the condition that the line l_1 passing through the points D and E and the line l_2 tangent to the ellipses S_1 and S_2 (the projections of the planes $\Pi_{1,2} \perp \mathbf{B}$ onto the plane $x + y = 0$) have the same inclination angle α (Fig. 19). The angle α shown in Fig. 19 is the angle of inclination of \mathbf{B} to the axis z and determines the position of the point Q .

As is easy to see, the equations of the ellipses S_1 and S_2 shown in Fig. 19 have the form

$$3(z - 1/2)^2 + 2w^2 = 2r^2$$

and

$$3(z - 1/2)^2 + 2(w - \sqrt{2})^2 = 2r^2$$

($w = (y - x)/\sqrt{2}$), respectively.

It can be seen that, on the one hand,

$$\tan \alpha = \frac{1/2 - r\sqrt{2/3}}{1/\sqrt{2} + r/\sqrt{3}} = \frac{\sqrt{3} - 2\sqrt{2}r}{\sqrt{6} + 2r}$$

(disappearance of the cylinder C_1).

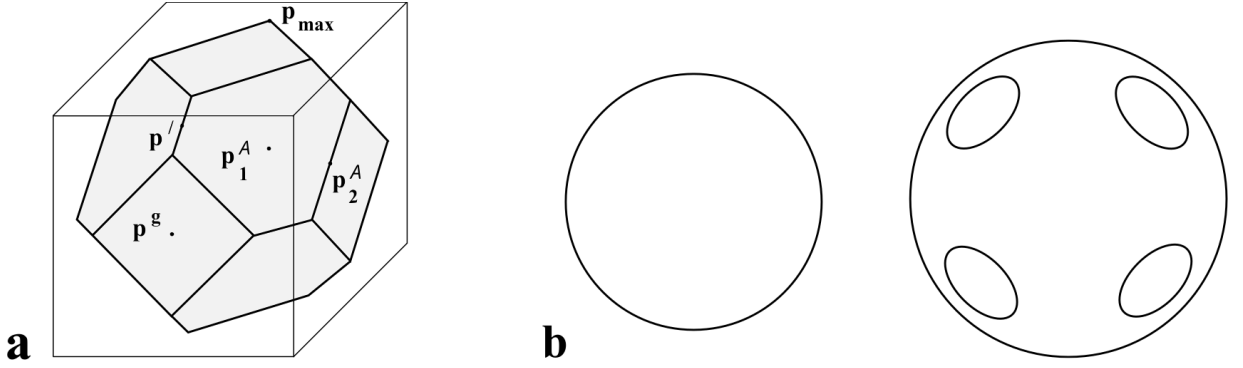


FIG. 17: (a) Brillouin zone for the face-centered cubic lattice (reciprocal lattice - body-centered cubic). (b) Surgery of the Fermi surface upon passing through $\epsilon_F = 3/4$.

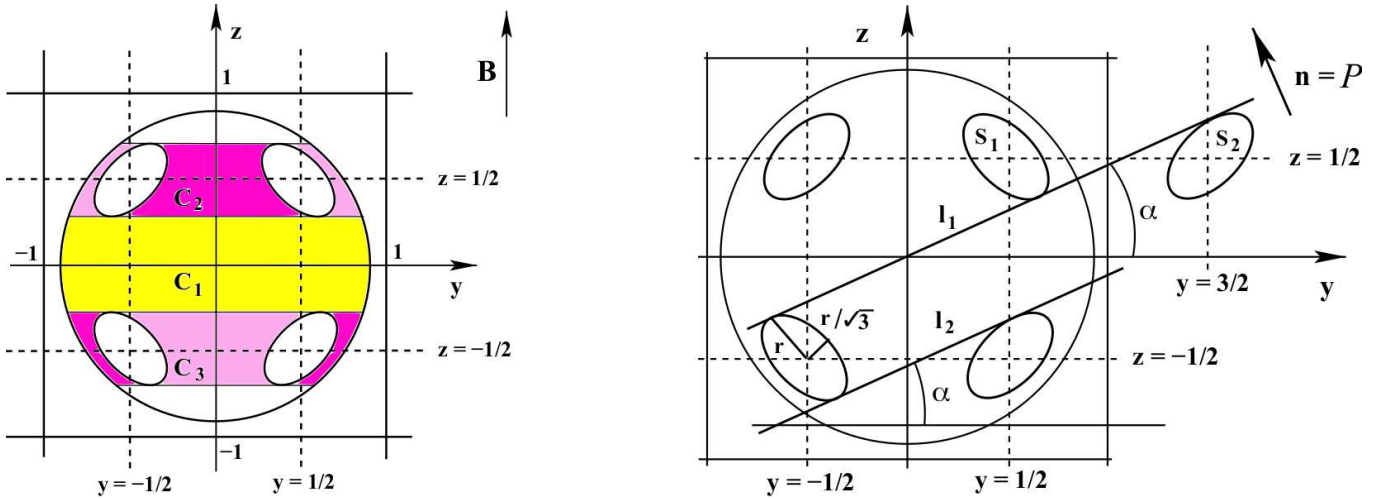


FIG. 18: Projection of the Fermi surface onto the yz plane for $\mathbf{B} \parallel z$ and disappearance of the cylinders C_1 , C_2 and C_3 for $\mathbf{n} = P$ (face-centered lattice).

On the other hand, the tangency condition of the line

$$(z - 1/2) = \tan \alpha (w - 1/\sqrt{2})$$

and the ellipses S_1 and S_2 leads to the relation

$$\tan \alpha = \frac{2r}{\sqrt{3 - 6r^2}}$$

The given relations result in

$$r(Q) \simeq 0.264889$$

$$\tan \alpha_Q \simeq 0.329890$$

$$\tilde{\epsilon}_0(Q) = \frac{3}{4} + r^2 \simeq 0.820166$$

Thus, for the case of the face-centered lattice, we can write

$$[\epsilon_1^B, \epsilon_2^B] \simeq [0.817, 0.820]$$

It can be seen that, according to our estimate, the interval $[\epsilon_1^B, \epsilon_2^B]$ lies in the energy region where the genus of the Fermi surface is 4, and the increase in the genus of S_F to 7 at $\epsilon_F = 1$ does not affect the emergence of ultra-complex angular diagrams.

Again abstracting from our normalization, we can say that, in the nearly free electron approximation for the face-centered cubic lattice, the interval of emergence of ultra-complex angular diagrams in the first conduction band lies at a distance of $\simeq 0.57 \epsilon_{\max}$ from its bottom and occupies $\simeq 0.2\%$ of the band width.

IV. THE BODY-CENTERED CUBIC LATTICE

In this section, we will consider the case of the body-centered cubic lattice. The reciprocal lattice in this case is face-centered cubic, and we will assume its edge length to be equal to 2. As in the previous case, we will be interested in the first conduction band in the nearly free

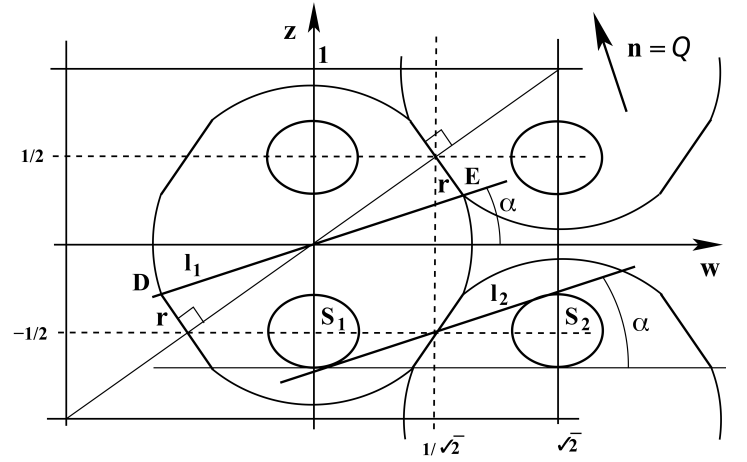
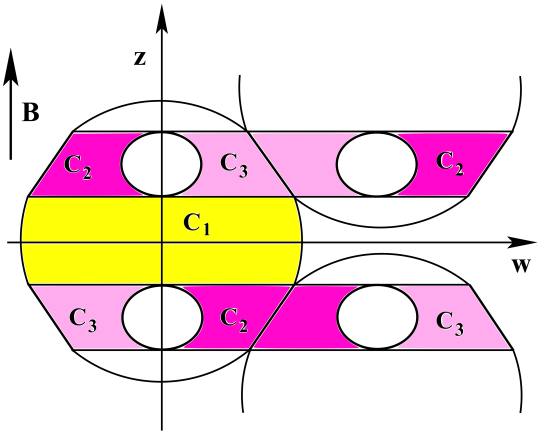


FIG. 19: Projection of the Fermi surface onto the plane $x + y = 0$ for $\mathbf{B} \parallel z$ and disappearance of the cylinders C_1 , C_2 and C_3 for $\mathbf{n} = Q$ (face-centered lattice).

electron approximation.

The emergence of the first (compact) components of the Fermi surface now occurs near integer points (m, n, l) of the \mathbf{p} -space, such that

$$m + n + l = 2s, \quad s \in \mathbb{Z}$$

As above, we will set

$$\Delta\epsilon(\mathbf{p}) = (\Delta\mathbf{p})^2$$

near these points.

The Brillouin zone now has the form shown in Fig. 20, a.

The Fermi surface remains spherical (in the torus \mathbb{T}^3) in the interval $\epsilon_F \in (0, 1/2)$.

The value

$$\epsilon_F = \epsilon_1^A = 1/2, \quad (p_1^A = 1/\sqrt{2}),$$

corresponds to the first touch of the spheres in \mathbf{p} -space (at the points p_1^A), after which the Fermi surface acquires genus 6 (Fig. 20, b).

At the value

$$\epsilon_F = \epsilon_2^A = 2/3, \quad (p_2^A = \sqrt{2/3}),$$

the spheres reach the edges of the Brillouin zone (at the points p_2^A), and the Fermi surface again decomposes into components of genus 0, which vanish at the values

$$\epsilon_F = \epsilon' = 3/4, \quad (p' = \sqrt{3}/2)$$

and

$$\epsilon_F = \epsilon_{\max} = 1, \quad (p_{\max} = 1)$$

We will, certainly, consider here the Fermi surfaces at $\epsilon_F \in [\epsilon_1^A, \epsilon_2^A]$ (Fig. 20, b).

As in the previous sections, we will be interested here in the values of $\tilde{\epsilon}_0(\mathbf{n})$ at the “symmetric” points of the boundary of W_1 (points P and Q , Fig. 8).

To determine the structure of system (I.1), as in the previous sections, we need to describe the cylinders of closed trajectories arising on the Fermi surface for $\mathbf{n} \in W_1$. Near the direction $\mathbf{n} \parallel z$, the number of such cylinders is 5, and they cut the Fermi surface into 4 tori with holes (carriers of open trajectories) $\mathbb{T}_{1,2,3,4}^2$, embedded in the three-dimensional torus

$$\mathbb{T}_{1,2,3,4}^2 \subset \mathbb{T}^2 = \mathbb{R}^3 / L^*$$

In the full \mathbf{p} -space, we then have 4 nonequivalent carriers of open trajectories, which are periodically deformed planes (with holes) parallel to the plane xy (Fig. 21).

The height of the cylinders of closed trajectories is maximal at $\mathbf{B} \parallel z$, and their structure is in many ways analogous to the structure for the face-centered lattice. In particular, here also arise (hole-type) cylinders C_2 and C_3 , completely analogous to the cylinders $C_{2,3}$ for the simple and face-centered lattices (see, e.g., Fig. 12, 18). As for the cylinder C_1 (Fig. 12, 18), now, due to the presence of additional “handles” (and a larger genus of the Fermi surface), it splits into two electron type cylinders C'_1 and C''_1 and a hole type cylinder C_0 (similar to cylinders C_2 and C_3).

Fig. 22 shows the arrangement of cylinders C_j on the Fermi surface in \mathbf{p} -space for $\mathbf{B} \parallel z$. Fig. 21 also shows the connection of the cylinders C_j with the carriers of open trajectories \mathbb{T}_i^2 for directions of \mathbf{B} close to the direction z .

It is easy to see that, when \mathbf{B} is deflected toward the point P , the cylinders C_2 and C_3 (they have a smaller height) disappear before the cylinder C_0 . Thus, the point P on the boundary of Zone W_1 is determined by the disappearance of the cylinders C'_1 and C''_1 (of the

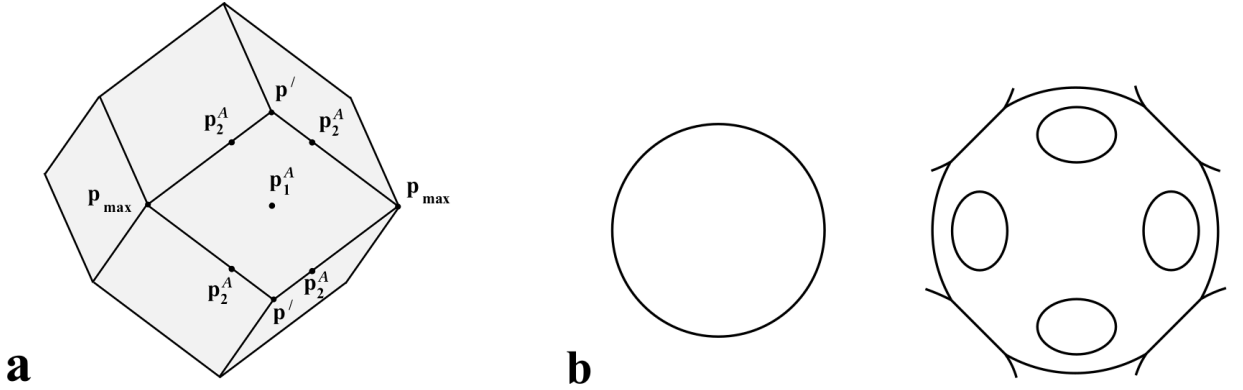


FIG. 20: (a) Brillouin zone for the body-centered cubic lattice (reciprocal lattice - face-centered cubic). (b) Surgery of the Fermi surface upon passing through $\epsilon_F = 1/2$.

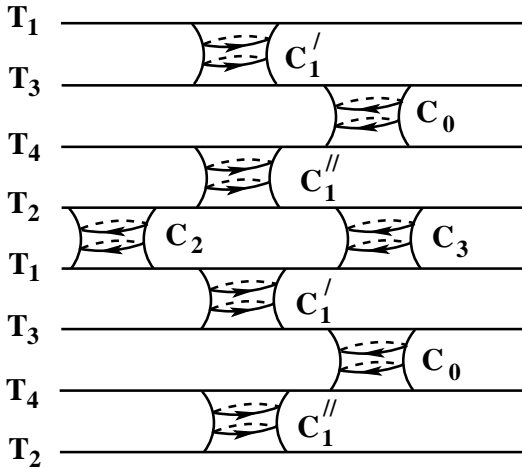


FIG. 21: "Scheme" of the connection of carriers of open trajectories and cylinders of closed trajectories near the direction $\mathbf{B} \parallel z$ (body-centered cubic lattice).

electron type) and the cylinder C_0 (of the hole type).

The disappearance of the cylinders C_1' , C_0 and C_1'' at $\mathbf{n} = P$ is shown in Fig. 22. The projections of the circles S_i onto the plane yz are now either segments of length $2r$ or ellipses with semi-axes r and $r/\sqrt{2}$. As is easy to see (Fig. 22), the equations of the projections of S_1 and S_2 have the form

$$2(y + 1/2)^2 + z^2 = r^2$$

and

$$2(y - 1/2)^2 + z^2 = r^2$$

respectively.

The position of the point P and the value $r(P)$ are determined by the equality of the inclination angles of the tangents (the projections of the planes $\Pi \perp \mathbf{B}$ onto the plane yz) to the projections of the circles S_i onto

the plane yz , as shown in Fig. 22. As can be verified, the condition of tangency of the line l_2 with the ellipses S_1 and S_2 has the form

$$\tan \alpha = \frac{2r}{\sqrt{1 - 2r^2}}$$

The line l_1 is given by the equation

$$z = \frac{2r}{\sqrt{1 - 2r^2}}(y + 1)$$

According to Fig. 22, it must contain the point

$$\left(\frac{1}{2} + \frac{r}{\sqrt{2}}, \frac{1}{2} - \frac{r}{\sqrt{2}} \right),$$

which implies

$$(1 - r\sqrt{2})\sqrt{1 - 2r^2} = 2r(3 + r\sqrt{2})$$

From the above relations we directly obtain

$$r(P) \simeq 0.126932$$

$$\tan \alpha_P \simeq 0.258056$$

$$\tilde{\epsilon}_0(P) \simeq 0.516112$$

Let us now consider the direction $\mathbf{n} = Q$. Fig. 23 shows the projection of the Fermi surface onto the plane $x + y = 0$. The projections of the circles S_i represent here either segments of length $2r$, or circles of radius r , or ellipses with semi-axes r and $r/2$. As is easy to see, the centers of the ellipses S_1 and S_2 lie at the points with coordinates

$$w = -\frac{1}{2\sqrt{2}}, \quad z = \frac{1}{2}$$

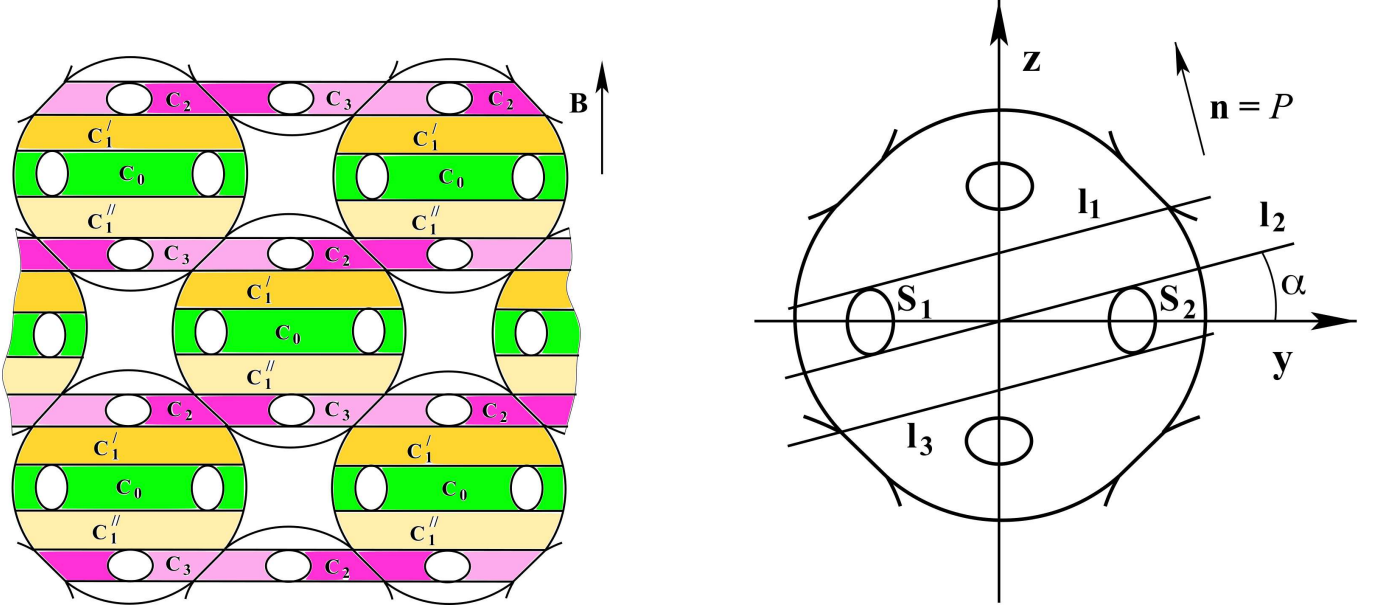


FIG. 22: Projections of cylinders of closed trajectories onto the plane yz for $\mathbf{B} \parallel z$ and the disappearance of cylinders C'_1 , C_0 and C''_1 for $\mathbf{n} = P$ (body-centered lattice).

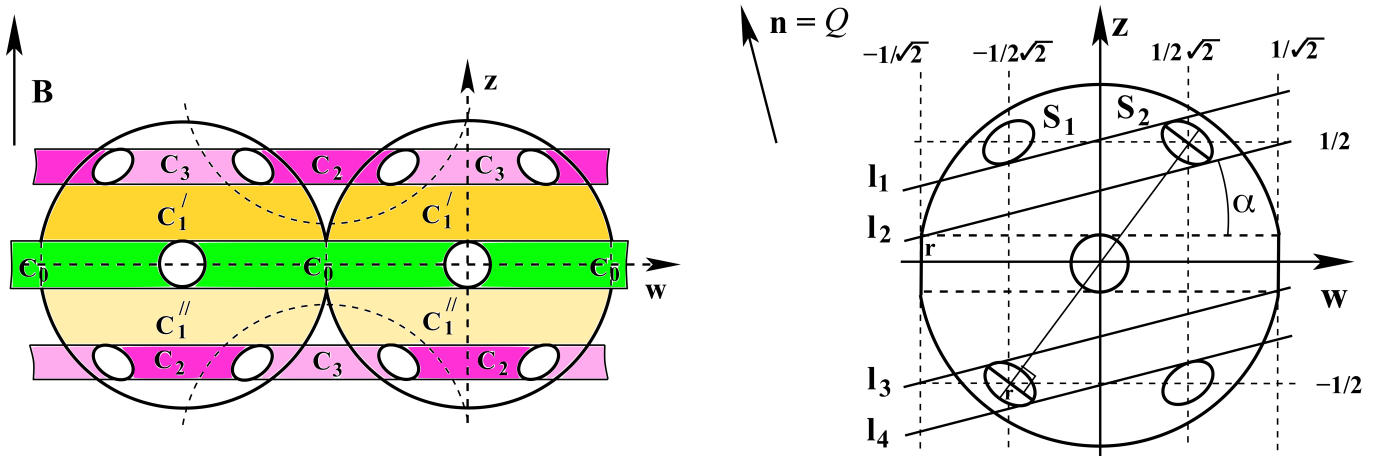


FIG. 23: Projections of cylinders of closed trajectories onto the plane $x + y = 0$ for $\mathbf{B} \parallel z$ and the disappearance of cylinders C'_1 , C''_1 , C_2 and C_3 for $\mathbf{n} = Q$ (body-centered lattice).

$$w = \frac{1}{2\sqrt{2}} \quad , \quad z = \frac{1}{2}$$

$$(w = (y - x)/\sqrt{2}).$$

As is not also difficult to show, the major semi-axes of the ellipses S_1 and S_2 are orthogonal to the segments connecting their centers with the origin.

Now it can be seen that, when \mathbf{B} is deflected towards the point Q , the cylinders C_0 (their projections onto the plane $x + y = 0$ have a much greater length) disappear before the cylinders C_2 and C_3 . Thus, the point Q on the boundary of Zone W_1 is determined by the disappearance of the cylinders C'_1 and C''_1 (of the electron

type) and the cylinders C_2 and C_3 (of the hole type).

As before, the projections of planes orthogonal to \mathbf{B} onto the plane $x + y = 0$ here represent lines with an inclination angle α with respect to the axis w . The condition for the simultaneous disappearance of the cylinders C'_1 , C''_1 , C_2 and C_3 is determined by the simultaneous tangency of the projections S_i by such lines, as shown in Fig. 23.

Ellipses S_1 and S_2 are given by the equations

$$4 \left(\sqrt{2}z - w - \frac{3}{2\sqrt{2}} \right)^2 + (z + \sqrt{2}w)^2 = 3r^2$$

and

$$4 \left(\sqrt{2}z + w - \frac{3}{2\sqrt{2}} \right)^2 + \left(z - \sqrt{2}w \right)^2 = 3r^2$$

respectively.

The equations of the lines l_1 and l_2 , as is not difficult to show, have the form

$$z = w \tan \alpha + 1 - \sqrt{2} \tan \alpha - r$$

and

$$z - r = \left(w + \frac{1}{\sqrt{2}} \right) \tan \alpha$$

As can be shown, the conditions for the correct tangency of the lines l_1 , l_2 and the ellipses S_1 , S_2 are given by the relations

$$\begin{aligned} \sqrt{2}r \sqrt{\left(\sqrt{2} + \tan \alpha \right)^2 + 4 \left(1 - \sqrt{2} \tan \alpha \right)^2} &= \\ &= 5\sqrt{3} \tan \alpha + 2\sqrt{6}r - \sqrt{6} \end{aligned}$$

and

$$\begin{aligned} \sqrt{2}r \sqrt{\left(\sqrt{2} - \tan \alpha \right)^2 + 4 \left(1 + \sqrt{2} \tan \alpha \right)^2} &= \\ &= \sqrt{6} - 3\sqrt{3} \tan \alpha - 2\sqrt{6}r, \end{aligned}$$

which implies

$$r(Q) \simeq 0.123591$$

$$\tan \alpha_Q = 0.255360$$

$$\tilde{\epsilon}_0(Q) \simeq 0.515275$$

Thus, for the case of the body-centered lattice, we can write

$$[\epsilon_1^B, \epsilon_2^B] \simeq [0.5153, 0.5161]$$

Abstracting from our normalization, we can say that, in the nearly free electron approximation for the body-centered cubic lattice, the interval of emergence of ultra-complex angular diagrams in the first conduction band lies at a distance of $\simeq 0.515 \epsilon_{\max}$ from its bottom and occupies $\simeq 0.1\%$ of the band width.

V. CONCLUSION

We estimate the ranges of occurrence of ultra-complex conductivity diagrams in the nearly free electron approximation for metals with cubic symmetry. The results of the study show that the occurrence of such diagrams corresponds to extremely narrow energy intervals $\epsilon_F \in [\epsilon_1^B, \epsilon_2^B]$ inside the conduction band, which coincides with similar estimates in the tight binding approximation ([44]). In our opinion, the obtained results are largely explained by the high symmetry of the crystal lattices, as well as the simplest analytical properties of the relations $\epsilon(\mathbf{p})$ considered in these studies. In particular, we expect wider ranges of occurrence of ultracomplex angular conductivity diagrams for conductors with more complex relations $\epsilon(\mathbf{p})$. In general, to observe ultra-complex angular conductivity diagrams, external influences on the crystal, shifting the position of ϵ_F within the conductivity band, are probably necessary.

[1] C. Kittel, Quantum Theory of Solids, Wiley, New York (1963)

[2] J.M. Ziman, Principles of the Theory of Solids, Cambridge University Press 1972.

[3] N.W. Ashcroft y N. D. Mermin, Solid State Physics, Saunders Collage Publishing, 1976.

[4] A.A. Abrikosov., Fundamentals of the Theory of Metals., Elsevier Science & Technology, Oxford, United Kingdom, 1988

[5] I.M. Lifshitz, M.Ya. Azbel, M.I. Kaganov., The Theory of Galvanomagnetic Effects in Metals., *Sov. Phys. JETP* **4**:1, 41-53 (1957).

[6] I.M. Lifshitz, V.G. Peschansky., Galvanomagnetic characteristics of metals with open Fermi surfaces., *Sov. Phys. JETP* **8**:5, 875-883 (1959).

[7] I.M. Lifshitz, V.G. Peschansky., Galvanomagnetic characteristics of metals with open Fermi surfaces. II., *Sov. Phys. JETP* **11**:1, 131-141 (1960).

[8] I.M. Lifshitz, M.Ya. Azbel, M.I. Kaganov., Electron Theory of Metals. New York: Consultants Bureau, 1973.

[9] S.P. Novikov., The Hamiltonian formalism and a many-valued analogue of Morse theory., *Russian Math. Surveys* **37** (5), 1-56 (1982).

[10] A.V. Zorich., A problem of Novikov on the semiclassical motion of an electron in a uniform almost rational magnetic field., *Russian Math. Surveys* **39** (5), 287-288 (1984).

[11] I.A. Dynnikov., Proof of S.P. Novikov's conjecture for the case of small perturbations of rational magnetic fields., *Russian Math. Surveys* **47**:3, 172-173 (1992).

[12] S.P. Tsarev, private communication, 1992-1993

[13] I.A. Dynnikov., Proof of S.P. Novikov's conjecture on the semiclassical motion of an electron., *Math. Notes* **53**:5, 495-501 (1993).

[14] A.V. Zorich., Proc. "Geometric Study of Foliations", (Tokyo, November 1993) / ed. T.Mizutani et al. Singapore: World Scientific, 479-498 (1994).

[15] I.A. Dynnikov., Surfaces in 3-torus: geometry of plane sections., *Proc. of ECM2, BuDA*, 1996.

[16] I.A. Dynnikov., Semiclassical motion of the electron. A proof of the Novikov conjecture in general position and counterexamples., *Solitons, geometry, and topology: on the crossroad*, Amer. Math. Soc. Transl. Ser. 2, 179, Amer. Math. Soc., Providence, RI, 1997, 45-73.

[17] I.A. Dynnikov., The geometry of stability zones in Novikov's problem on the semiclassical motion of an electron., *Russian Math. Surveys* **54**:1, 21-59 (1999).

[18] A. Ya. Maltsev and S. P. Novikov, Quasiperiodic functions and dynamical systems in quantum solid state physics, *Bulletin of Braz. Math. Society*, New Series **34**, 171 (2003).

[19] A. Ya. Maltsev and S. P. Novikov, Dynamical Systems, Topology, and Conductivity in Normal Metals, *J. Stat. Phys.* **115**, 31 (2004).

[20] A.Ya. Maltsev, S.P. Novikov, Topological integrability, classical and quantum chaos, and the theory of dynamical systems in the physics of condensed matter, *Russ. Math. Surv.*, **74**(1), 141-173 (2019)

[21] S.P. Novikov, A.Y. Maltsev., Topological quantum characteristics observed in the investigation of the conductivity in normal metals., *JETP Letters* **63** (10), 855-860 (1996).

[22] A.Ya. Maltsev, The second boundaries of stability zones and the angular diagrams of conductivity for metals having complicated Fermi surfaces, *Journal of Experimental and Theoretical Physics* **127** (6), 1087-1111 (2018)

[23] A.Ya. Maltsev, The Complexity Classes of Angular Diagrams of the Metal Conductivity in Strong Magnetic Fields, *Journal of Experimental and Theoretical Physics* **129**(1), 116-138 (2019)

[24] A.Ya. Maltsev., Anomalous behavior of the electrical conductivity tensor in strong magnetic fields., *Journal of Experimental and Theoretical Physics* **85** (5), 934-942 (1997)

[25] A.Ya. Maltsev, S.P. Novikov., The Theory of Closed 1-Forms, Levels of Quasiperiodic Functions and Transport Phenomena in Electron Systems., *Proceedings of the Steklov Institute of Mathematics* **302**, 279-297 (2018).

[26] Anton Zorich., How do the leaves of closed 1-form wind around a surface., "Pseudoperiodic Topology", V.I.Arnold, M.Kontsevich, A.Zorich (eds.), Translations of the AMS, Ser. 2, vol. 197, AMS, Providence, RI, 1999, 135-178.

[27] R. De Leo., Existence and measure of ergodic leaves in Novikov's problem on the semiclassical motion of an electron., *Russian Math. Surveys* **55**:1 (2000), 166-168.

[28] R. De Leo., Characterization of the set of "ergodic directions" in Novikov's problem of quasi-electron orbits in normal metals., *Russian Math. Surveys* **58**:5 (2003), 1042-1043.

[29] R. De Leo., Topological effects in the magnetoresistance of Au and Ag., *Phys. Lett. A* **332**, 469-474 (2004)

[30] R. De Leo., First-principles generation of stereographic maps for high-field magnetoresistance in normal metals: An application to Au and Ag., *Physica B: Condensed Matter* **362** (1-4) (2005), 62-75.

[31] R. De Leo., Topology of plane sections of periodic polyhedra with an application to the Truncated Octahedron., *Experimental Mathematics* **15**:1 (2006), 109-124.

[32] R. De Leo, I.A. Dynnikov., An example of a fractal set of plane directions having chaotic intersections with a fixed 3-periodic surface., *Russian Math. Surveys* **62**:5 (2007), 990-992.

[33] I.A. Dynnikov, Interval identification systems and plane sections of 3-periodic surfaces, *Proceedings of the Steklov Institute of Mathematics* **263**, 65-77 (2008).

[34] R. De Leo, I.A. Dynnikov., Geometry of plane sections of the infinite regular skew polyhedron $\{4, 6 | 4\}$., *Geom. Dedicata* **138**:1 (2009), 51-67.

[35] A. Skripchenko., Symmetric interval identification systems of order three., *Discrete Contin. Dyn. Sys.* **32**:2 (2012), 643-656.

[36] A. Skripchenko., On connectedness of chaotic sections of some 3-periodic surfaces., *Ann. Glob. Anal. Geom.* **43** (2013), 253-271.

[37] I. Dynnikov, A. Skripchenko., On typical leaves of a measured foliated 2-complex of thin type., *Topology, Geometry, Integrable Systems, and Mathematical Physics: Novikov's Seminar 2012-2014, Advances in the Mathematical Sciences*, Amer. Math. Soc. Transl. Ser. 2, 234, eds. V.M. Buchstaber, B.A. Dubrovin, I.M. Krichever, Amer. Math. Soc., Providence, RI, 2014, 173-200, arXiv: 1309.4884

[38] I. Dynnikov, A. Skripchenko., Symmetric band complexes of thin type and chaotic sections which are not actually chaotic., *Trans. Moscow Math. Soc.*, Vol. 76, no. 2, 2015, 287-308.

[39] A. Avila, P. Hubert, A. Skripchenko., Diffusion for chaotic plane sections of 3-periodic surfaces., *Inventiones mathematicae*, October 2016, Volume 206, Issue 1, pp 109-146.

[40] A. Avila, P. Hubert, A. Skripchenko., On the Hausdorff dimension of the Rauzy gasket., *Bulletin de la societe mathematique de France*, 2016, **144** (3), pp. 539 - 568.

[41] Roberto De Leo., A survey on quasiperiodic topology., *Advanced Mathematical Methods in Biosciences & Applications*, Springer, Eds. F. Berezovskaya and B. Toni, (2018)., arXiv:1711.01716

[42] Ivan Dynnikov, Pascal Hubert, Alexandra Skripchenko, Dynamical Systems Around the Rauzy Gasket and Their Ergodic Properties, *International Mathematics Research Notices IMRN* 2022, 1-30 (Published online), arXiv 2011.15043

[43] I.A. Dynnikov, A.Ya. Maltsev, S.P. Novikov, Geometry of quasi-periodic functions on the plane, *Russian Math. Surveys* **77** : 6, 1061-1085 (2022), arXiv:2306.11257

[44] A.Ya. Maltsev, On chaotic regimes of conductivity behavior in the tight-binding approximation, arXiv:2510.17589

[45] Walter A. Harrison, Electronic Structure of Polyvalent Metals, *Phys. Rev.* **118**, 1190 (1960).